Chapter 3: *Deep Convection* Lead Author: Jean Philippe Lafore, CNRM-GAME, Météo-France

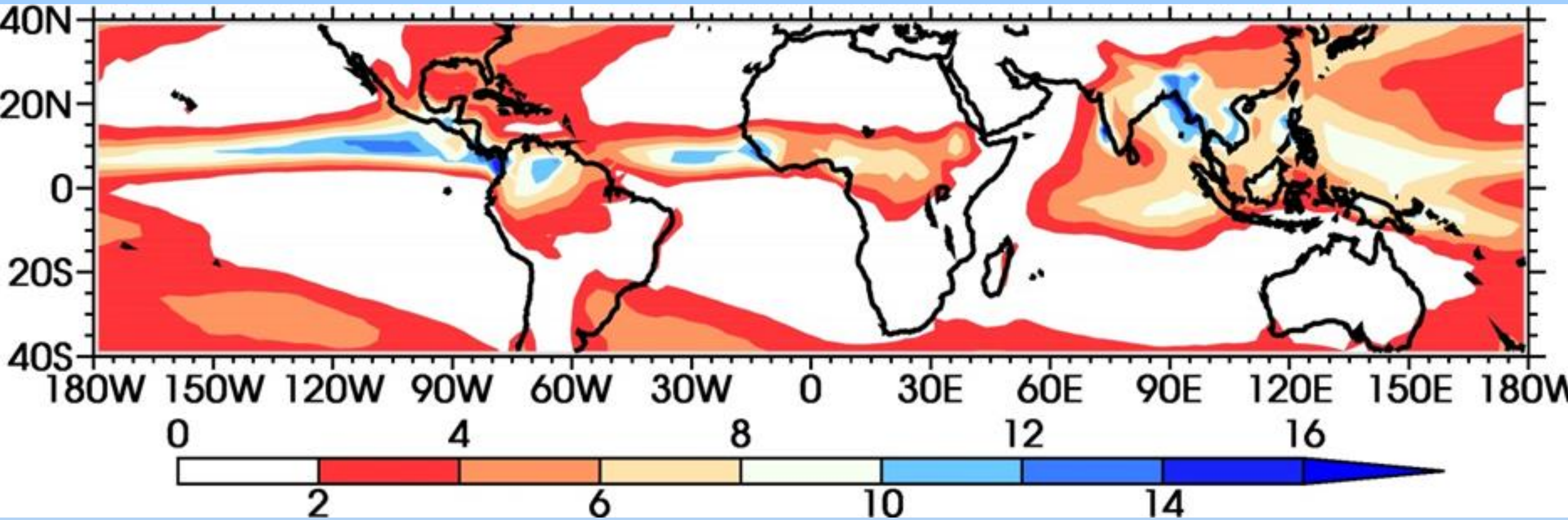

Figure 3.1: Boreal summer (JJAS) mean distribution of rainfall (mm/day) over the tropics for the 1979-2012 period, based on GPCP version 2.2 monthly precipitation dataset . **JPL COMMENT: TO BE REPLOTTED** (Adler et al. 2003)

Chapter 3: *Deep Convection* Lead Author: Jean Philippe Lafore, CNRM-GAME, Météo-France

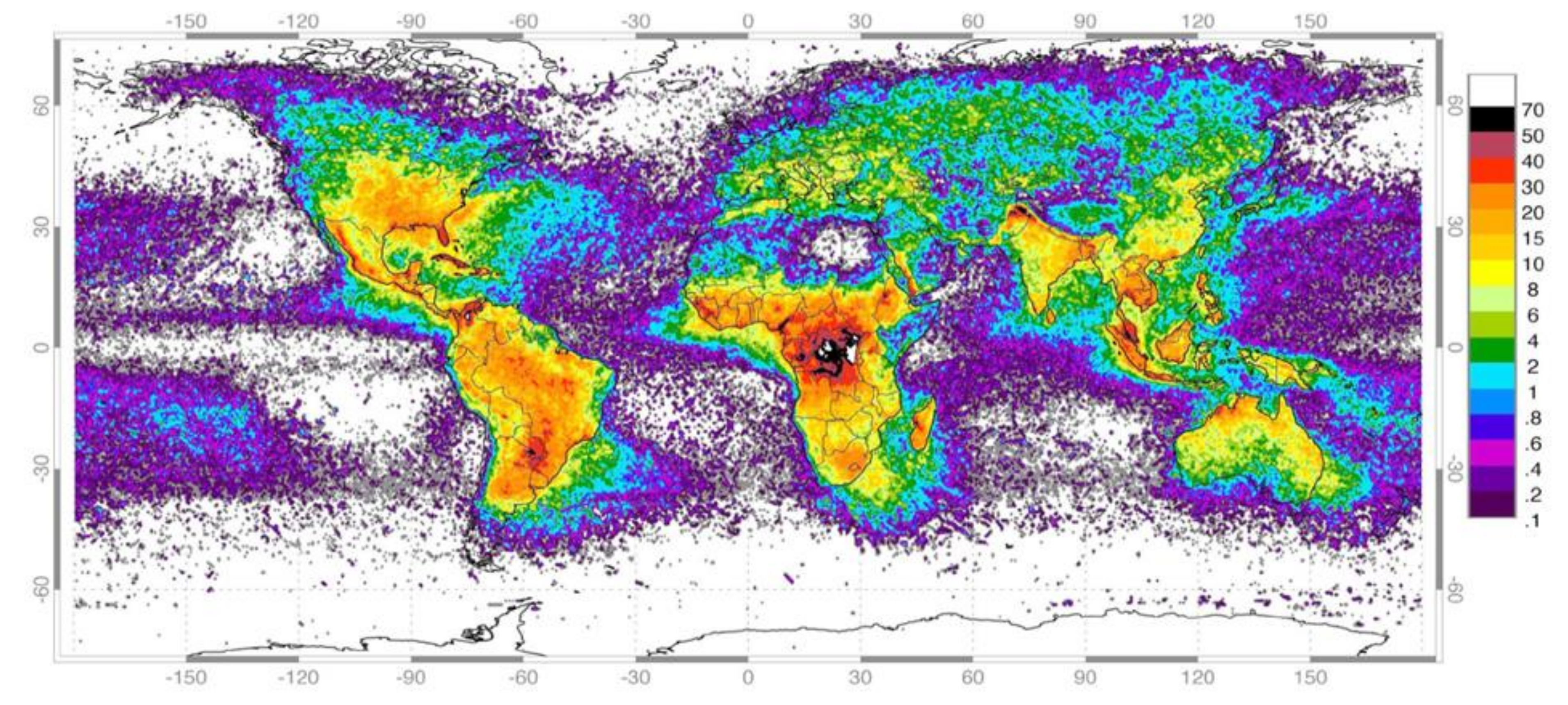

Figure 3.2: Annual number of lightning flashes by pixel over the 1995-2003 period.
(after Global Hydrology Resources Center)

African Monsoon Multidisciplinary Analysis

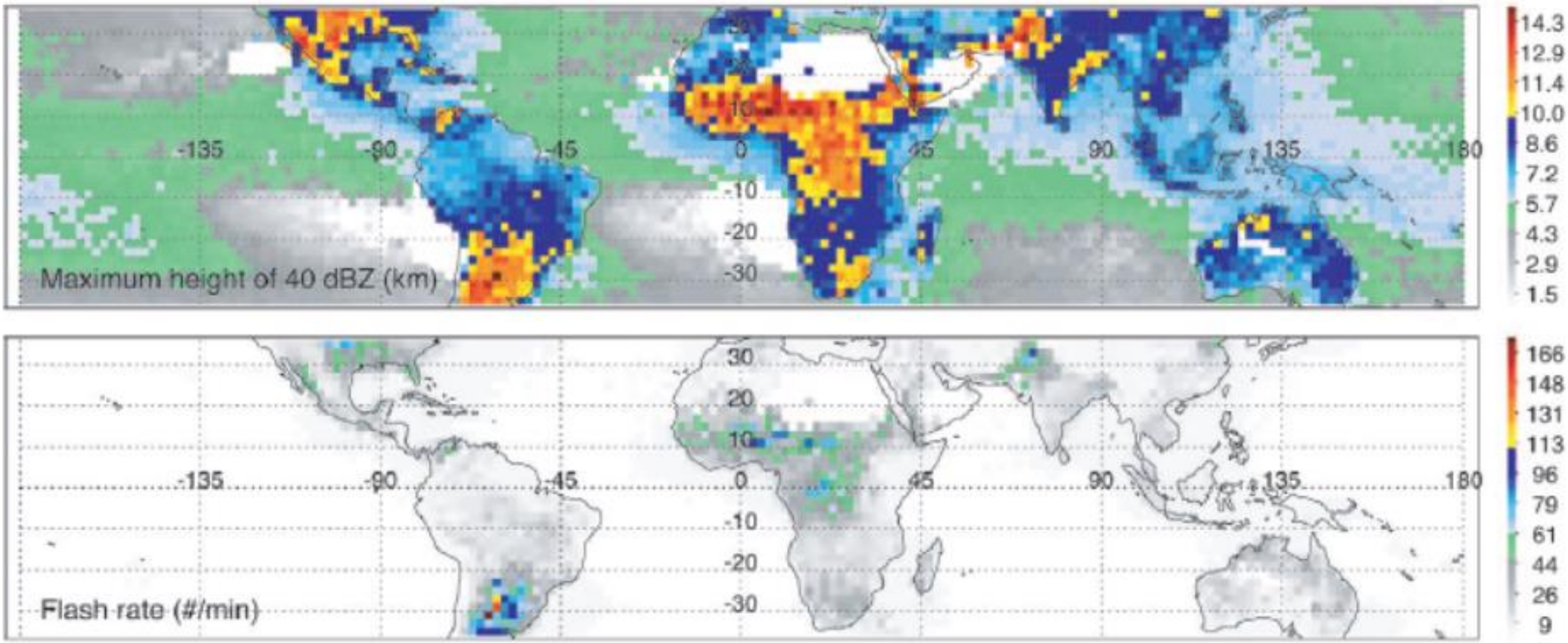

Figure 3.3: Distribution of the most extreme storms (1% precipitation features - PF) for each 2◦ latitude x 2◦ longitude box, for: (a) the maximum height (km) and (b) the flash rate (/min). Boxes with less than 150 PFs are left blank.
(after Zipser et al., 2006)

African Monsoon Multidisciplinary Analysis

Chapter 3: *Deep Convection* Lead Author: Jean Philippe Lafore, CNRM-GAME, Météo-France

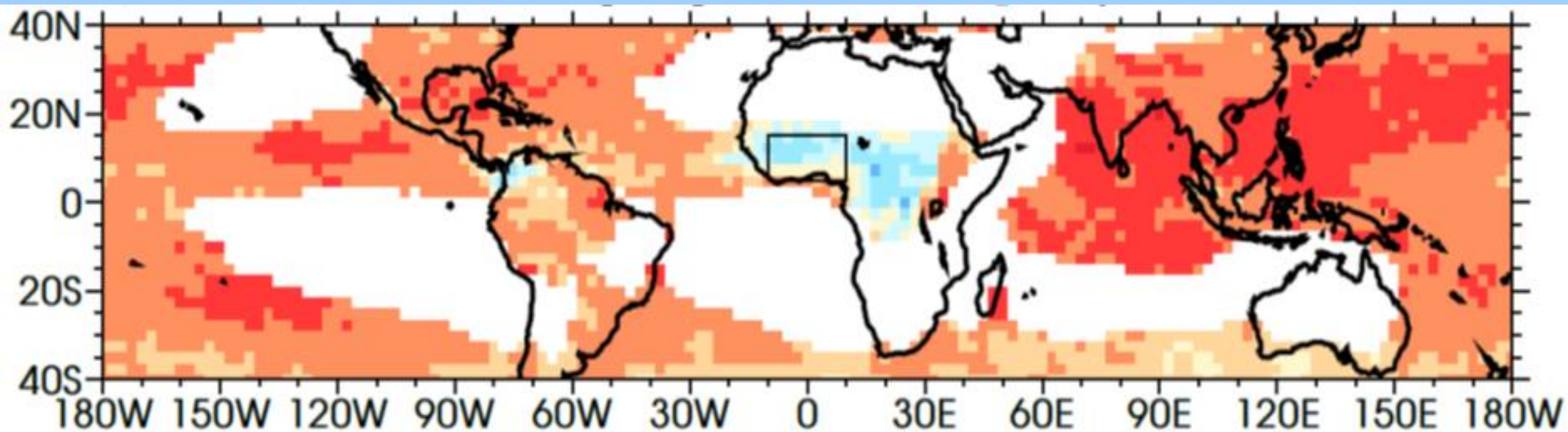

Figure 3.4: Autocorrelation of GPCP precipitation anomalies at a 1-day lag in JAS, for the 1997-2006 period).
(after Roehrig et al., 2013)

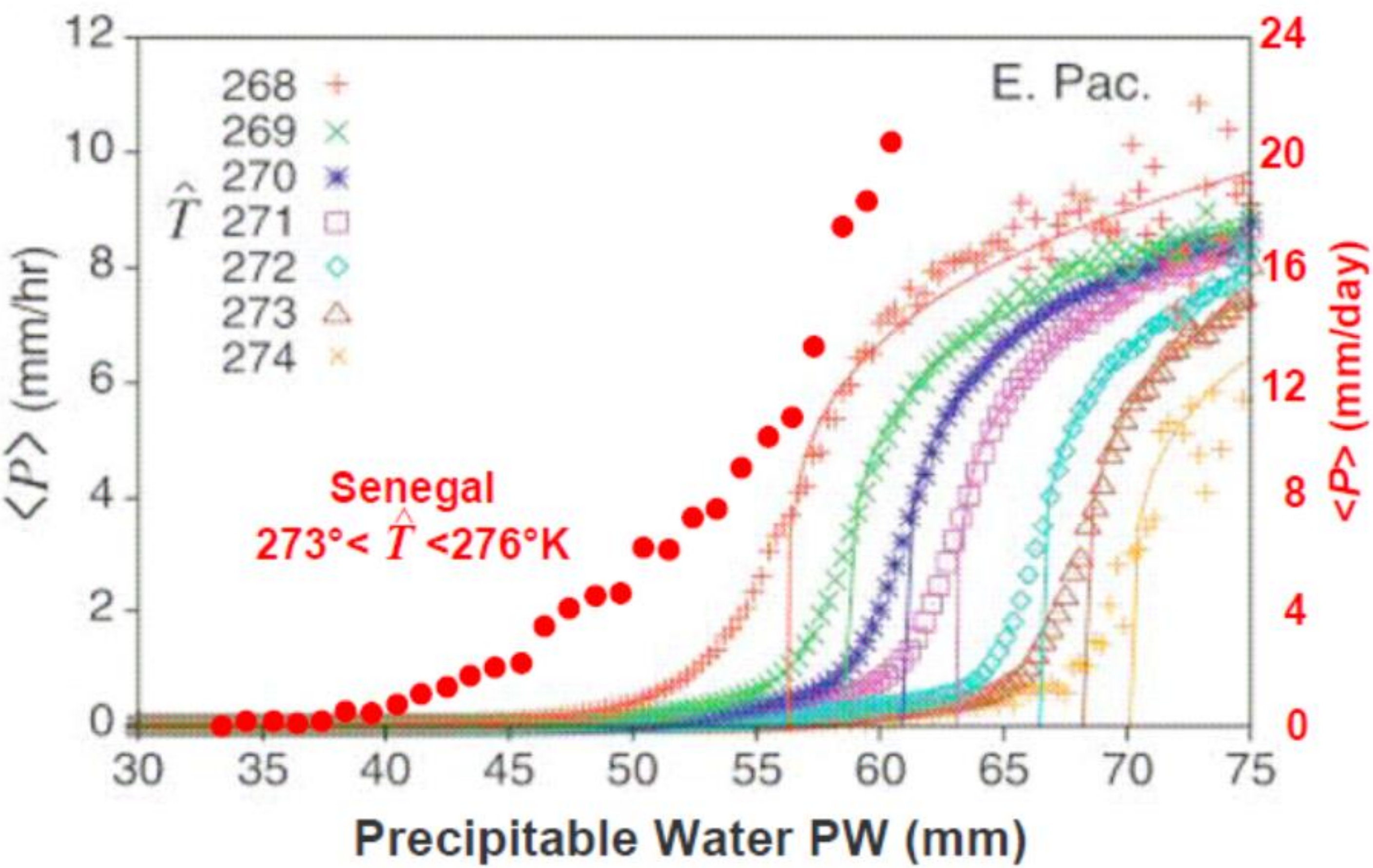

Figure 3.5: Observed average precipitation rate <P> (in mm/hr) as a function of precipitable water (PW in mm), for the eastern Pacific for 1◦K bins of the vertically averaged tropospheric temperature (After Neelin et al., 2009). Daily precipitation rates <P> (in mm/day) observed by the Senegal raingauge network for the 2000-2011 period, have been superposed with red points.

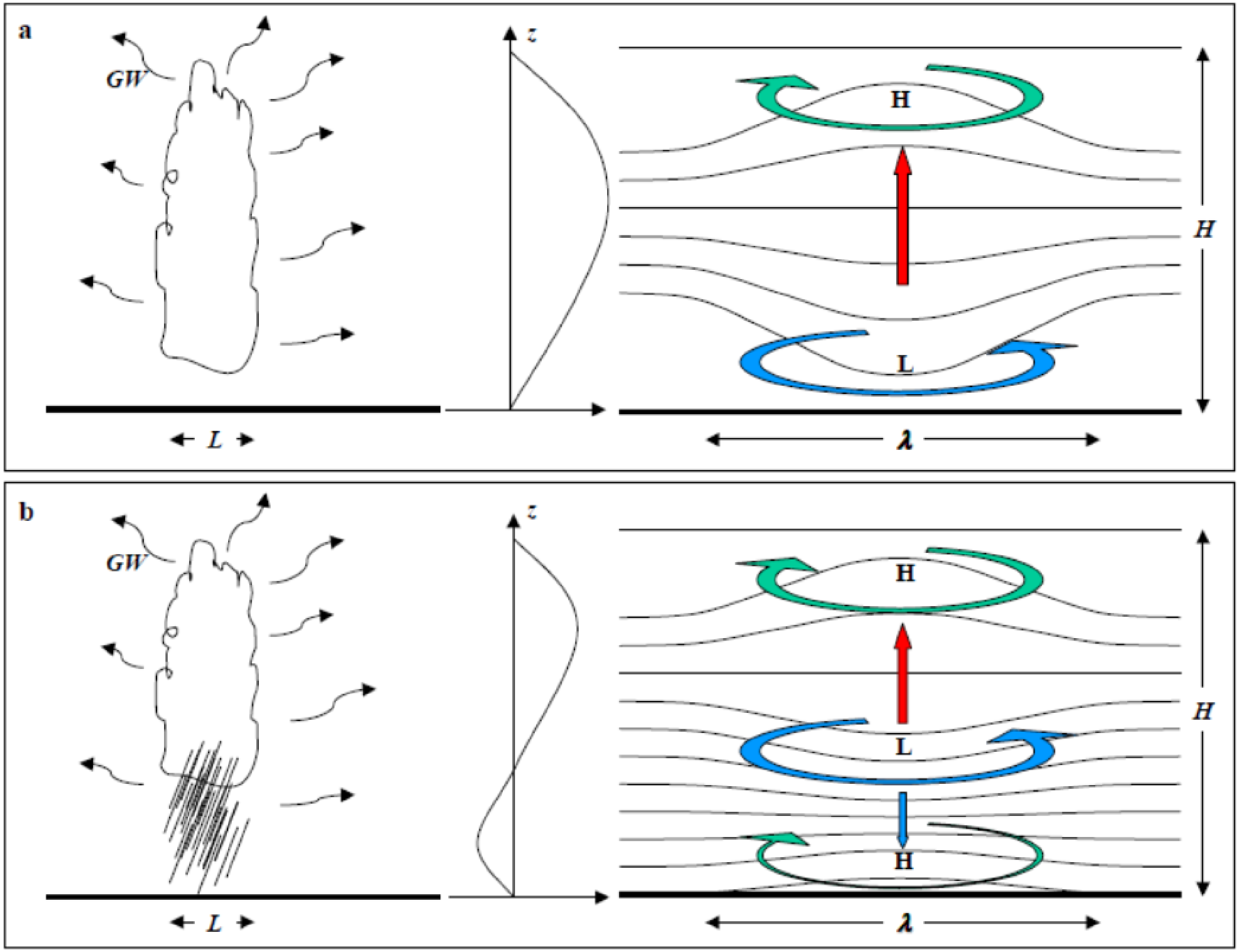

Figure 3.6: Schematic representation of the "Adjustment Problem" for (a) a simple convective heating profile, and (b) a convective cooling-heating vertical dipole, as typically observed for semi-arid conditions characterized by an elevated cloud base.
Left side is the vertical structure of convective cells with characteristic horizontal L and vertical H scales, emitting gravity waves (GW) in the stable environment. The corresponding vertical cooling-heating profiles are provided in the middle.
Right side represents the resulting geostrophic equilibrium reached after a ~1/f time scale for the geopotential height field, and the associated mean vertical motion, cyclonic and anticyclonic circulations at the scale of the Rossby radius λ.

Chapter 3: *Deep Convection* Lead Author: Jean Philippe Lafore, CNRM-GAME, Météo-France

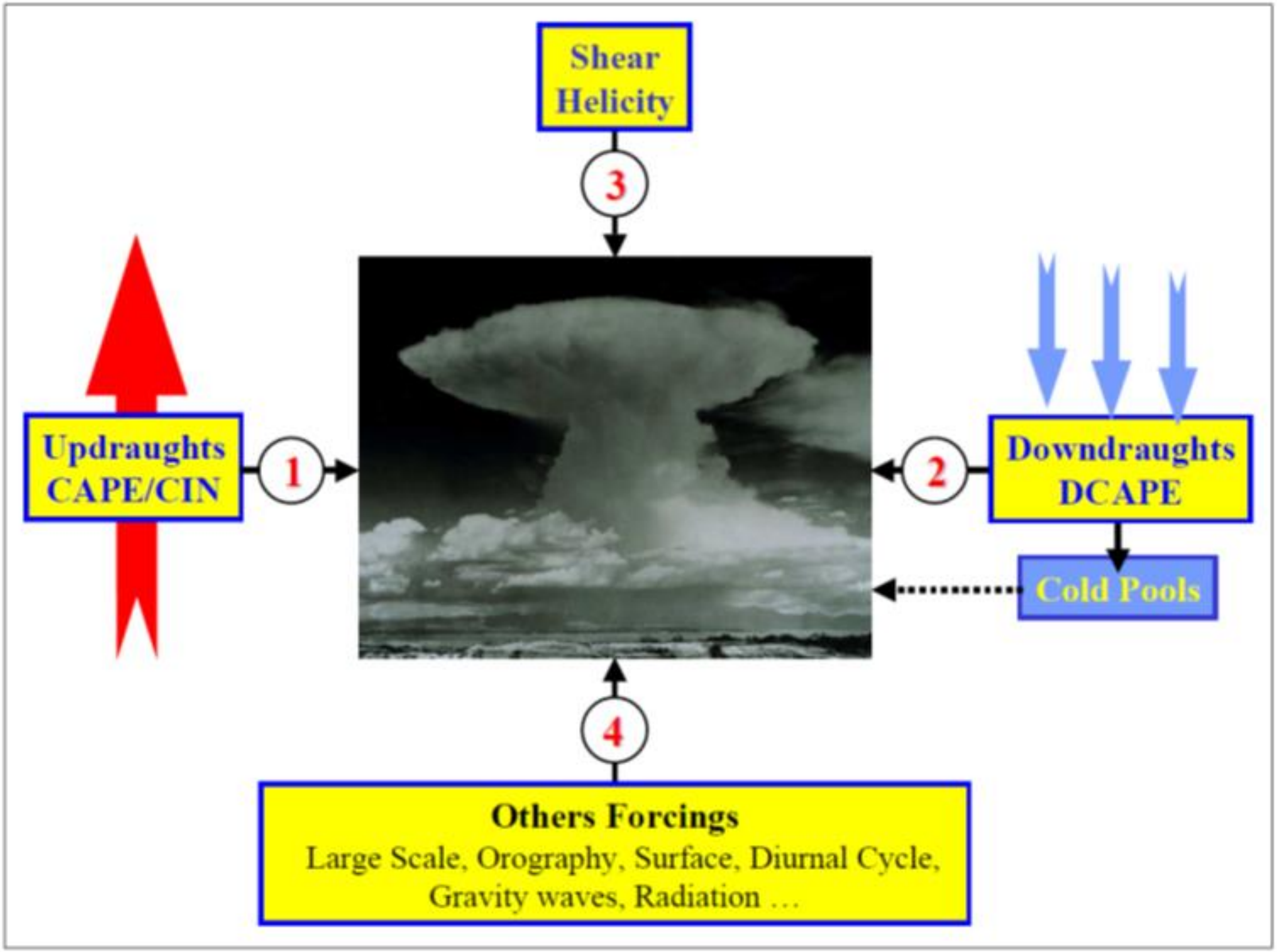

Figure 3.7: Schematic representation of the 4 types of processes and related indices that govern the convective activity.

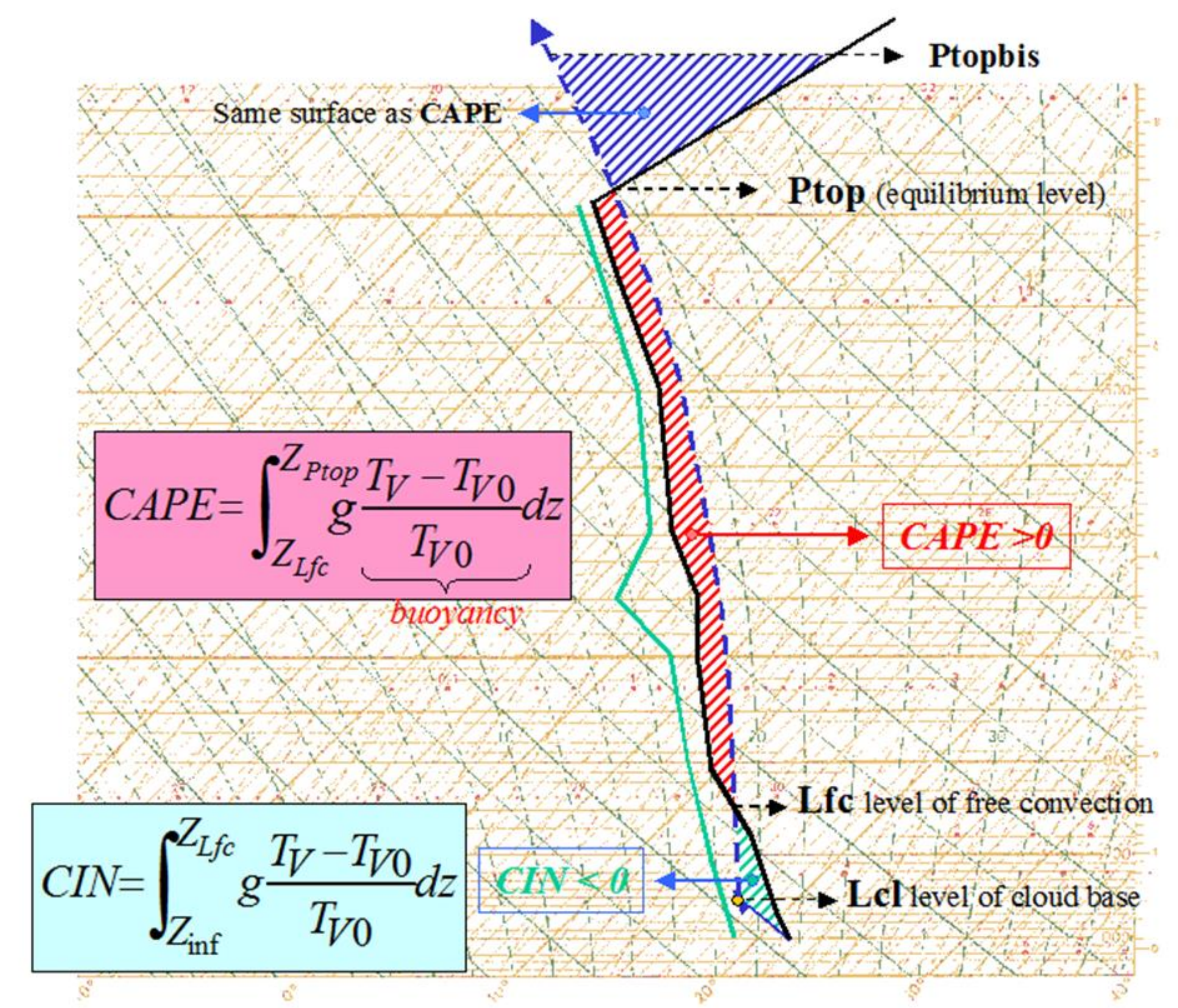

Figure 3.8: Illustration of the Parcel theory for an air mass lifted from the surface.

JPL COMMENT: FIGURE TO BE REDRAWN

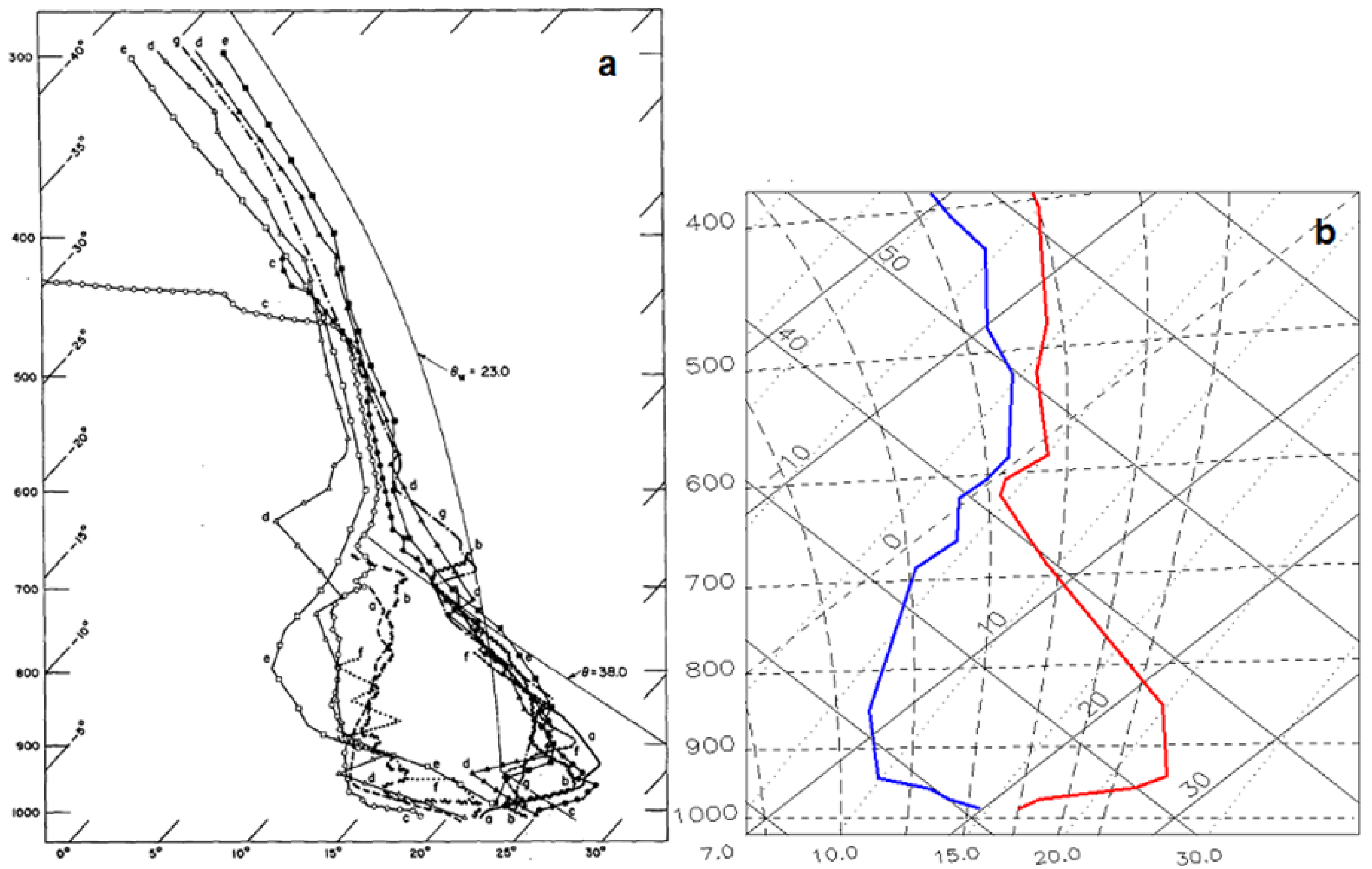

Figure 3.9: Characteristic soundings in postquall regions illustrating the impact of mesoscale subsidences: (a) for Caribbean and GATE squall-lines (After Zipser, 1977), and (b) an African one observed at Niamey during the AMMA SOP on 22 July 2006 at 12:00UTC.

Chapter 3: *Deep Convection* Lead Author: Jean Philippe Lafore, CNRM-GAME, Météo-France

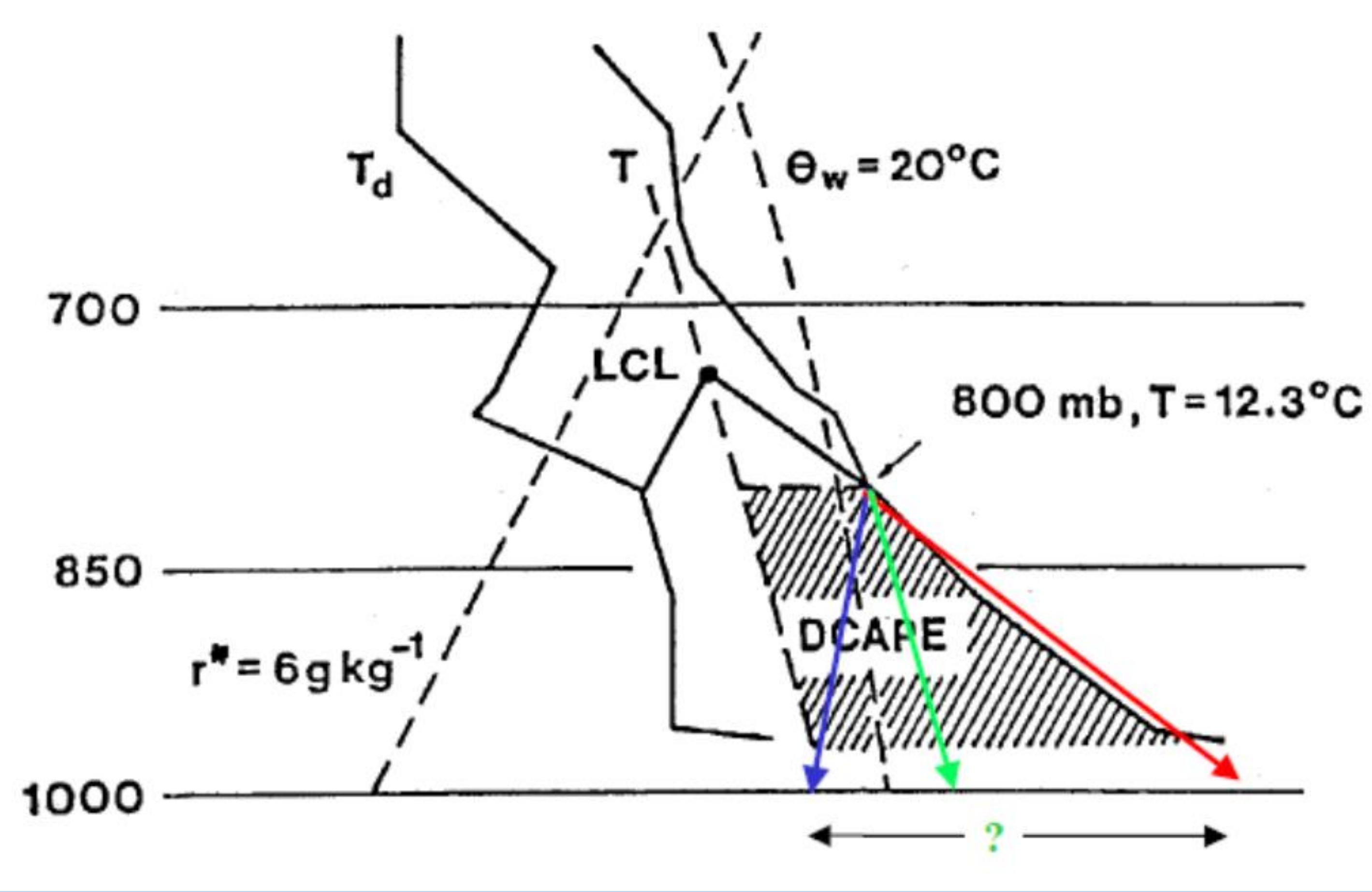

Figure 3.10: Illustration of the computation of the DCAPE index on a tephigram, for a subsiding parcel taken at 800 hPa. The blue arrow indicates the descent of air which reaches the ground completely saturated; the red arrow denotes dry adiabatic descent, and the green arrow represents the most common occurrence, lying between the moist and dry extremes. Therefore there is considerable uncertainty in the temperature of the downdraught at ground level.

African Monsoon Multidisciplinary Analysis

Chapter 3: ***Deep Convection*** **Lead Author: Jean Philippe Lafore, CNRM-GAME, Météo-France**

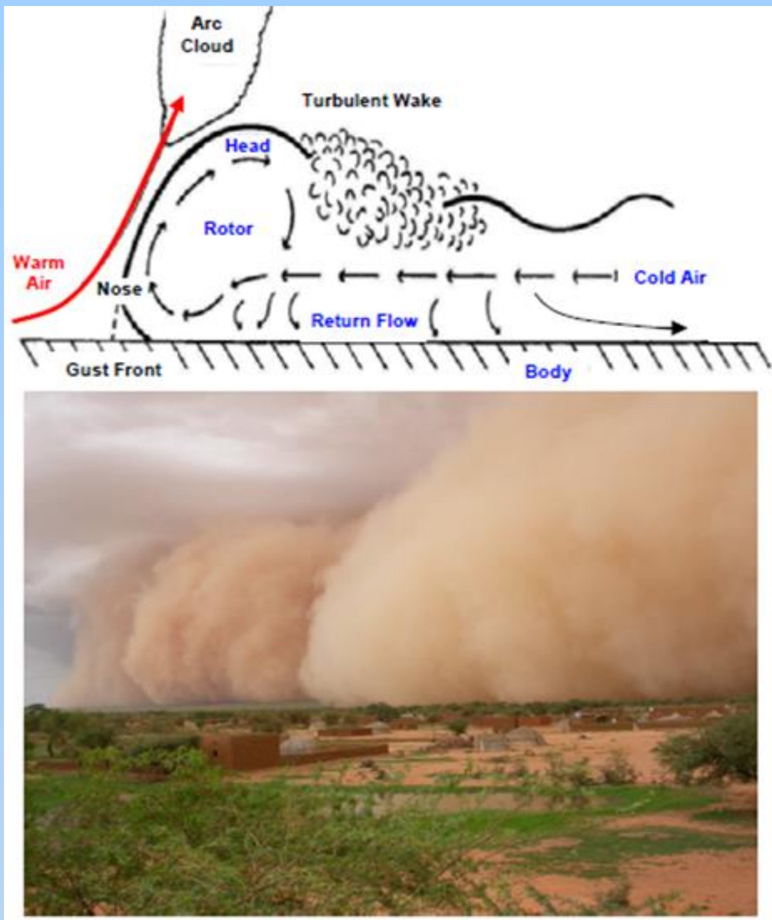

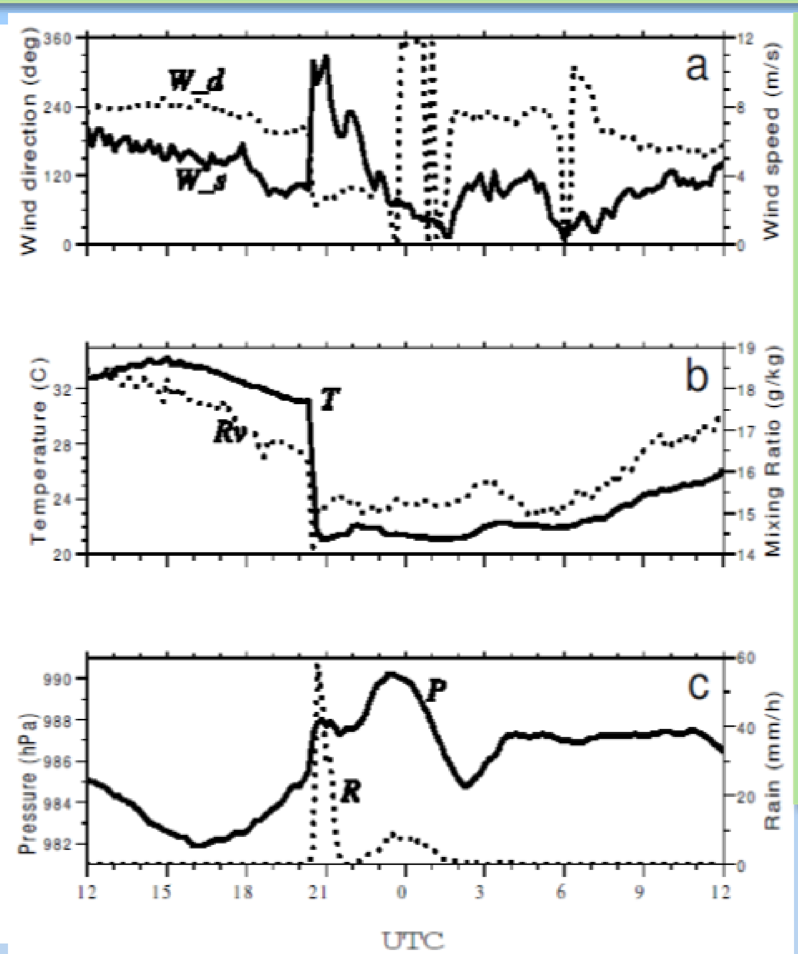

Figure 3.11: Left column: schematic view of a cold pool, and a picture of the arrival of a convective cold pool lifting dust, a phenomenon often referred to as haboob

(© CNRS Photothèque, by F. Guichard and L. Kergoat, Mali August 2004).

Figure 3.11: Right column: an example of the signature of a cold pool passage at the surface for a Sahelian squall line for (a) wind intensity and direction, the temperature T and vapour mixing ratio Rv, and (c) the surface pressure P and the precipitation intensity R (after Redelsperger et al., 2002).

African Monsoon Multidisciplinary Analysis

ACMAD

WMO

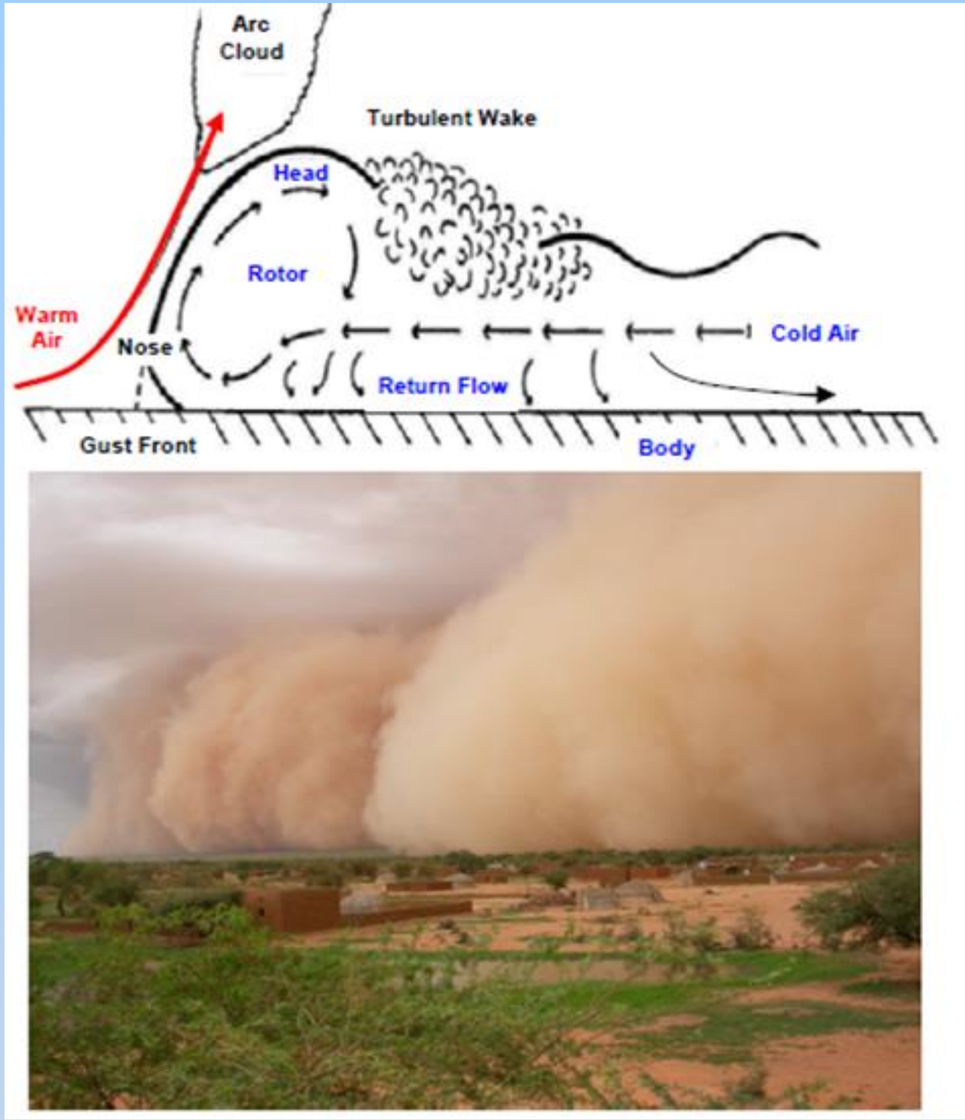

Figure 3.11: Left column: schematic view of a cold pool, and a picture of the arrival of a convective cold pool lifting dust, a phenomenon often referred to as haboob

(© CNRS Photothèque, by F. Guichard and L. Kergoat, Mali August 2004).

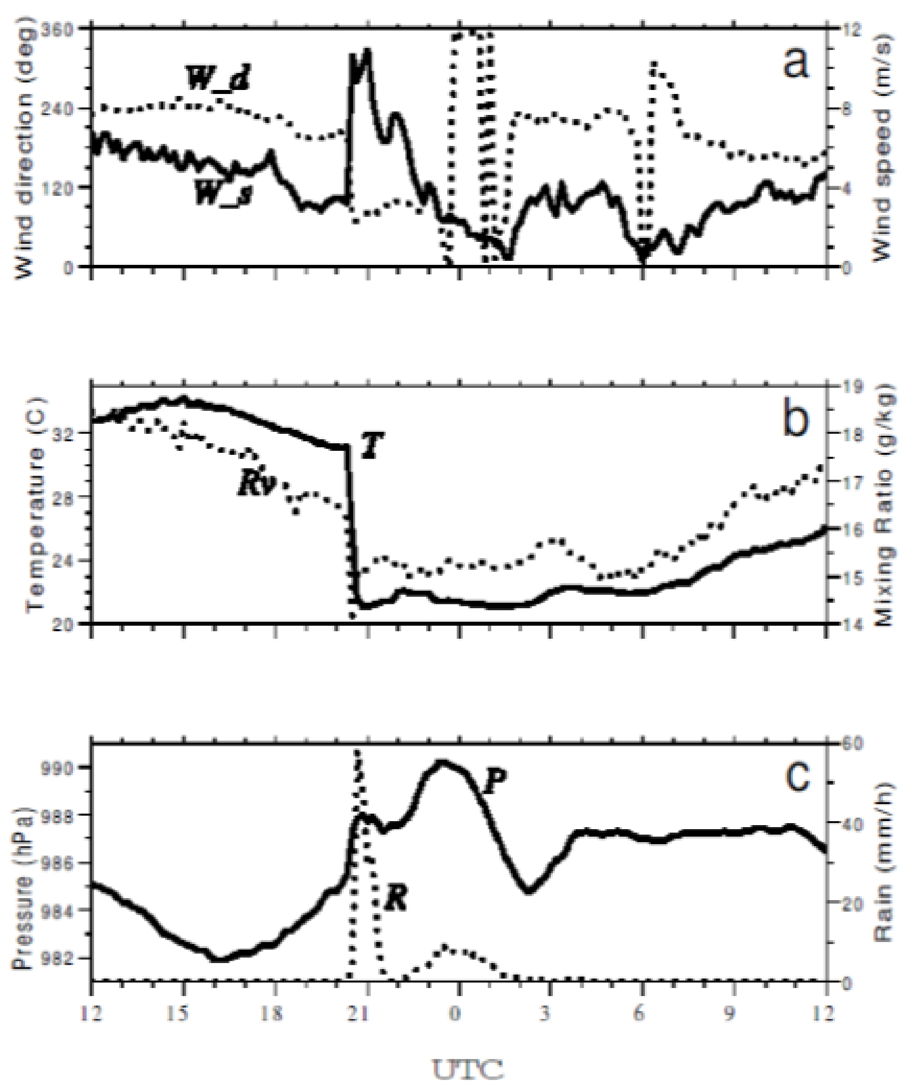

Figure 3.11: Right column: an example of the signature of a cold pool passage at the surface for a Sahelian squall line for (a) wind intensity and direction, the temperature T and vapour mixing ratio Rv, and (c) the surface pressure P and the precipitation intensity R (after Redelsperger et al., 2002).

African Monsoon Multidisciplinary Analysis

Chapter 3: *Deep Convection* Lead Author: Jean Philippe Lafore, CNRM-GAME, Météo-France

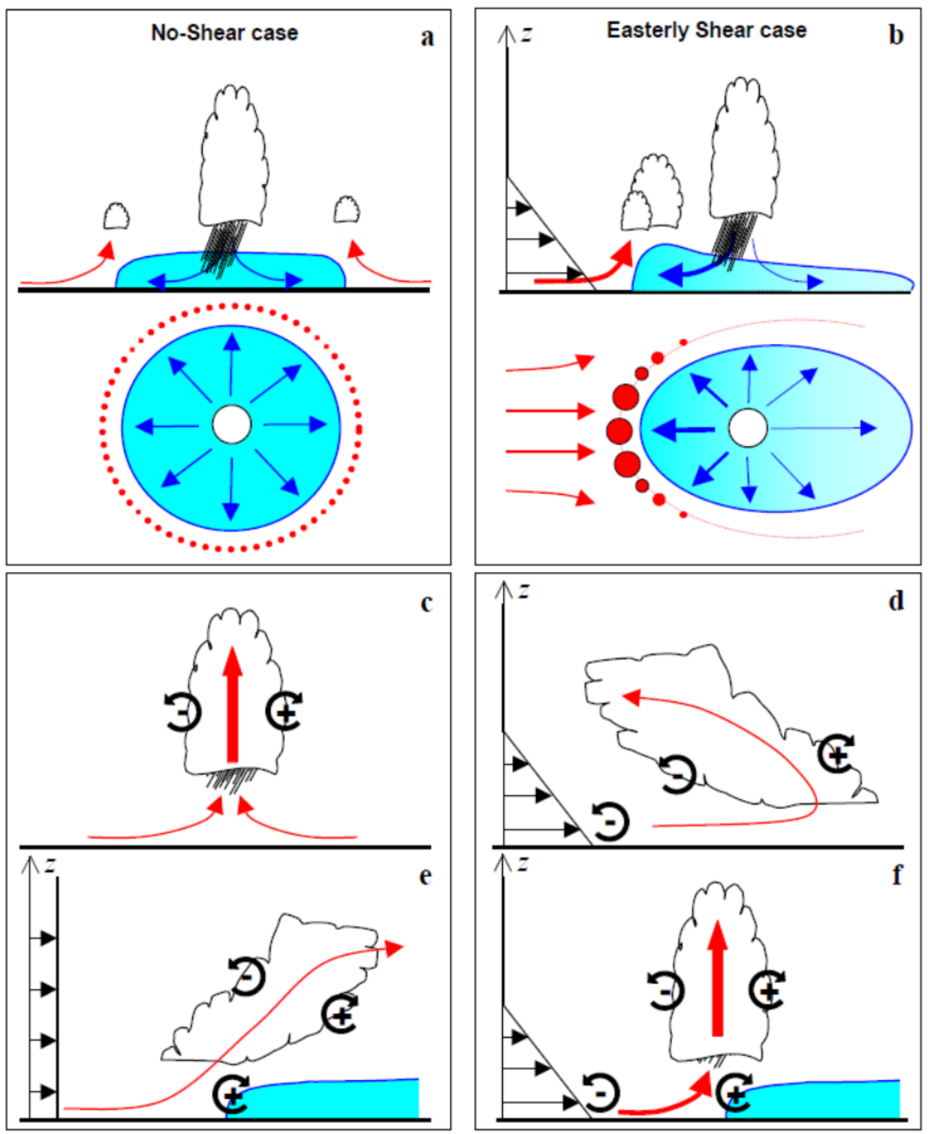

Figure 3.12: Schematic view of the impact of the shear on convection organisation in cases of no shear (left column) and of uni-directional easterly shear (right column).
Wind profiles in the environment are relative to the convection-cold pool system propagation. The upper row, (a) and (b), shows the impact of shear on a cold pool and its efficiency to lift new convective cells.
The lower two rows are a schematic diagram based on vorticity arguments showing how a buoyant updraught may be influenced by wind shear and/or a cold pool. (c) With no shear and no cold pool, the updraught axis produced by the thermally created, symmetric vorticity distribution is vertical. (d) With only shear, the distribution is biased toward negative vorticity and this causes the updraught to lean downshear. (e) With only a cold pool and no shear, the distribution is biased by positive vorticity of the underlying cold pool and causes the updraught to lean behind the cold pool. (f) With both a cold pool and shear, the two effects may negate each other, and allow an erect updraught.
(after Rotunno et al., 1988)

African Monsoon Multidisciplinary Analysis

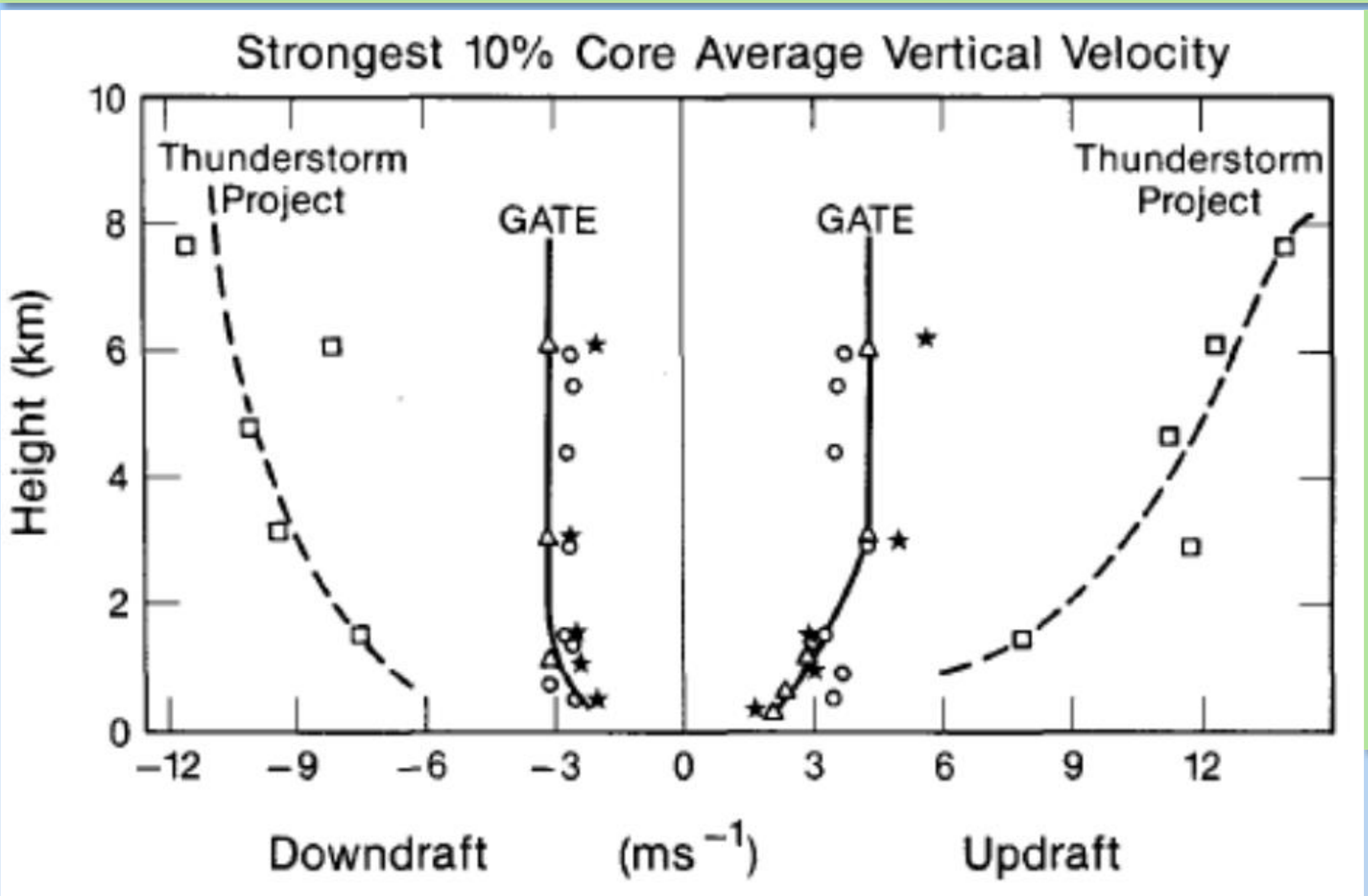

Figure 3.13: Observed strongest 10%-level average of vertical velocity in updraught and downdraught cores as function of height for GATE, TAMEX, hurricanes, EMEX and the Thunderstorm Project, corresponding to triangles, stars, circles, plus and squares respectively.

Adapted from Jorgensen and LeMone (1989) and Lucas et al. (1994).

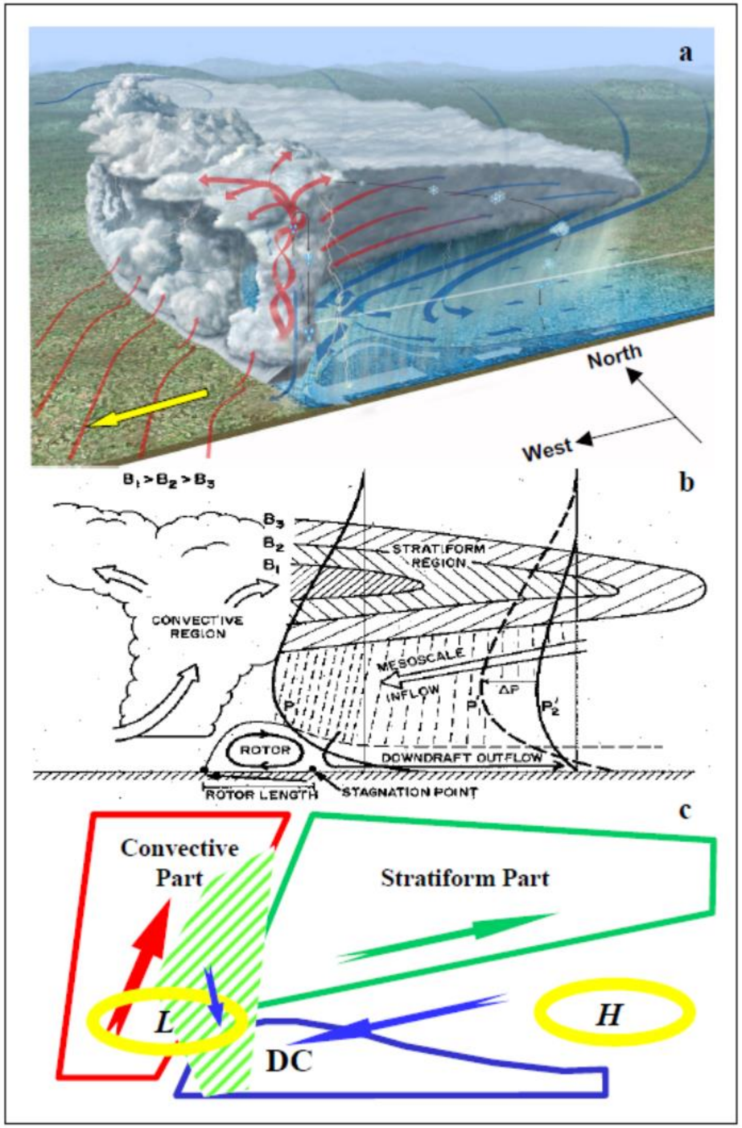

Figure 3.14: (a) 3D schematic view of a fast-moving squall line with the airflow circulation , the cold air mass forming the density current (DC) in blue shading, and some trajectories of hydrometeors. (b) 2D conceptual model of the squall line (adapted from Lafore and Moncrieff, 1989), and (c) its box representation.

(after Lafore 2004, ©François Poulain/Météo-France)

African Monsoon Multidisciplinary Analysis

ACMAD

WMO

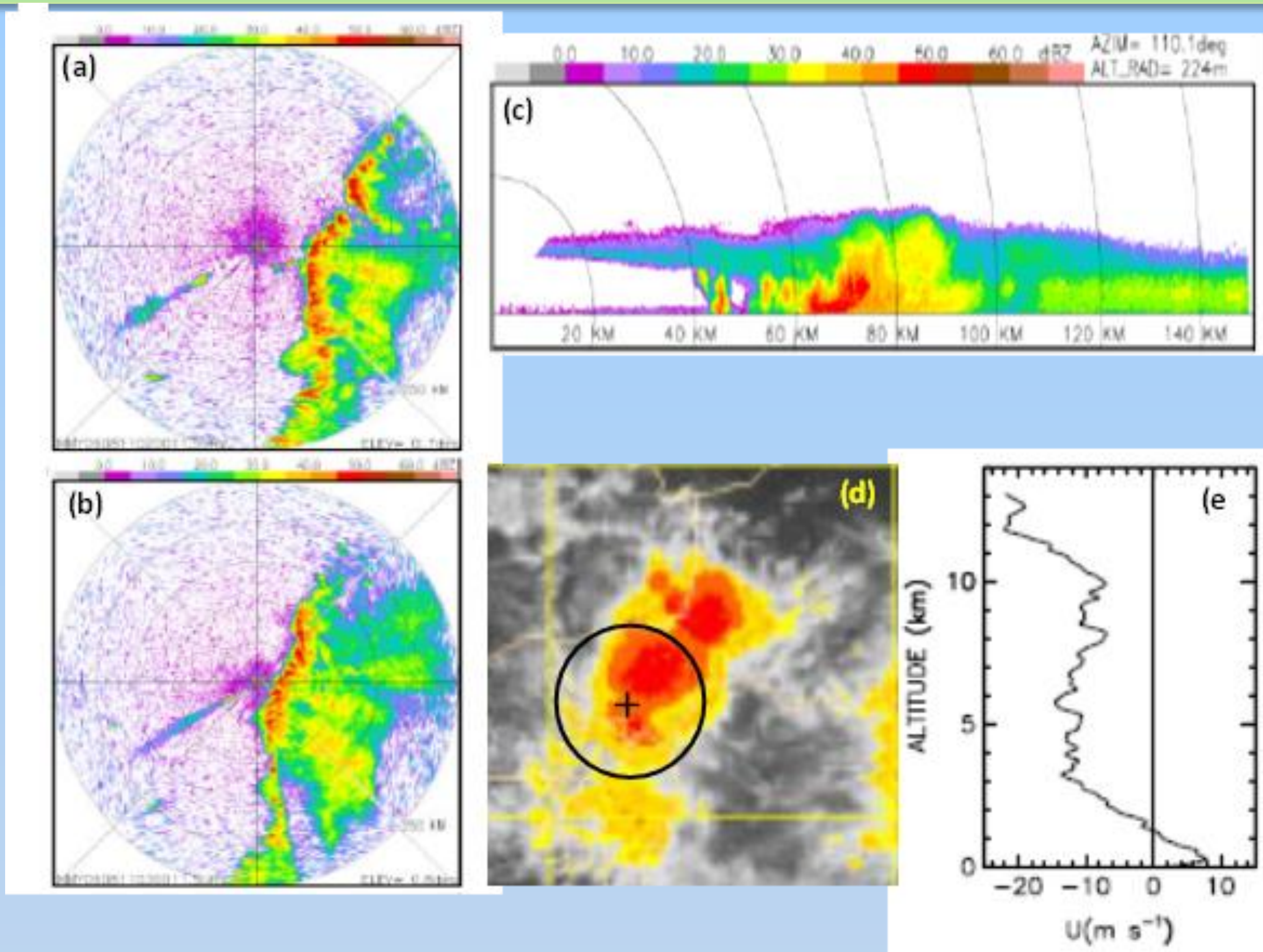

Figure 3.15: Squall line approaching Niamey (2.18°E, 13.48°N) on 11 August 2006 as seen by the MIT radar for reflectivity (dBZ) horizontal representation (PPI) at (a) 0200 and (b) 0300 UTC, and (c) a vertical cross section (RHI scan) at 0200 UTC. In (d), the radar range (250 km) is superposed on the IR Meteosat image at 0300 UTC and € shows the vertical profile of zonal wind observed a few hours before the squall line passage.

(after Lafore 2004, (after Chong, 2010)

Chapter 3: *Deep Convection* Lead Author: Jean Philippe Lafore, CNRM-GAME, Météo-France

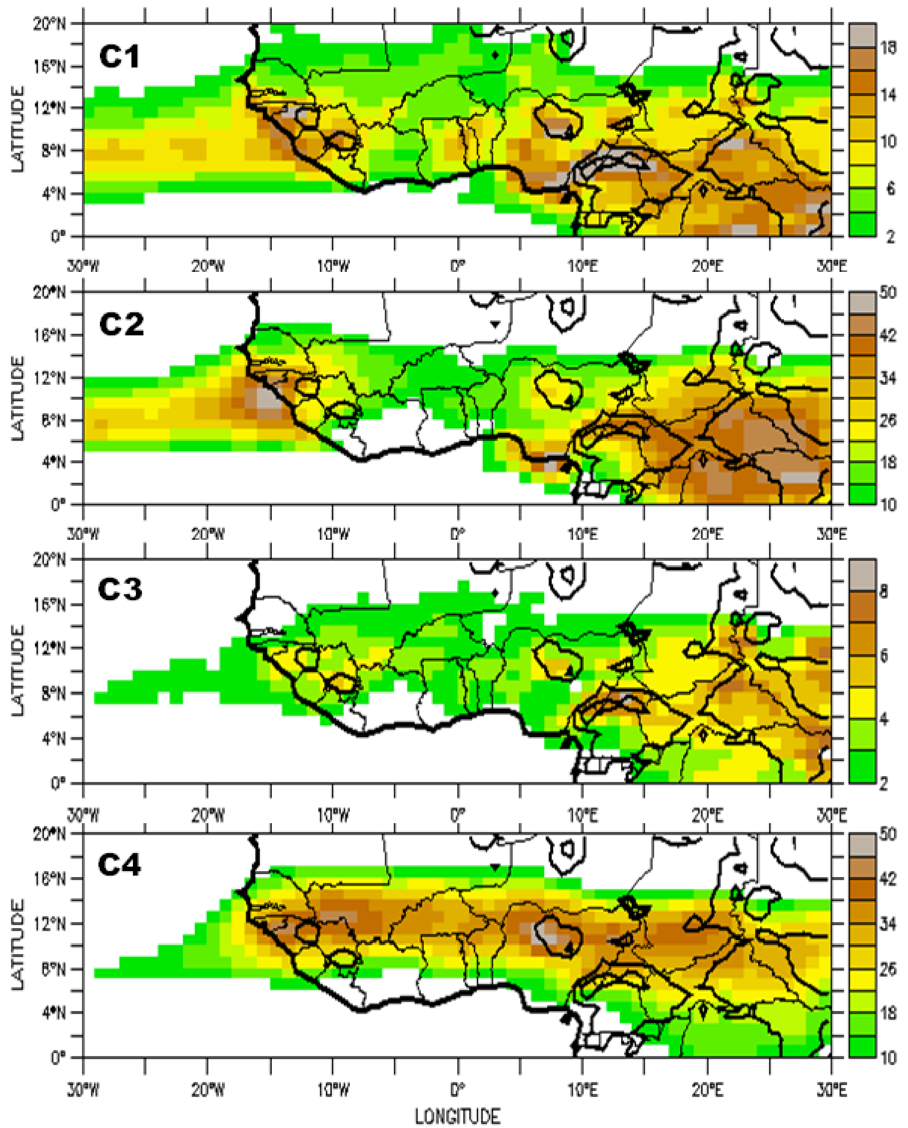

Figure 3.16: Spatial distribution of cloud cover JJAS climatology of MCSs over 25 years of Meteosat performed using the Fiolleau and Roca (2013) tracking algorithm for the 4 types of MCSs; C1, C2, C3 and C4 of the classification (see text). Resolution is 1° square and the unit is h/month. Heavy isolines represent surface altitude above 600 and 1200 m.

African Monsoon Multidisciplinary Analysis

ACMAD

WMO

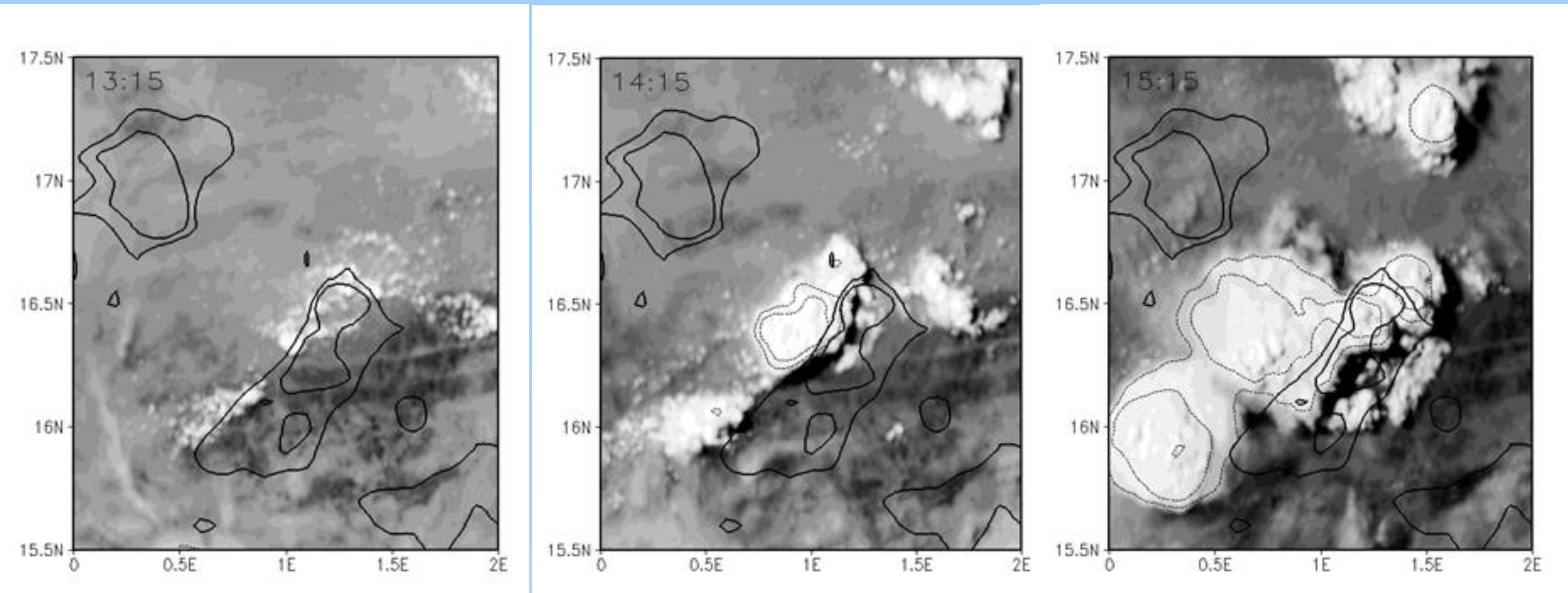

Figure 3.18: Example of the early afternoon development of a MCS in Mali from visible channel satellite data. Solid contours indicate wet patches created by rain the preceding day, and cloud top temperatures below -40 and -60°C are enclosed by dashed contours.
(after Taylor et al., 2010)

Chapter 3: *Deep Convection* Lead Author: Jean Philippe Lafore, CNRM-GAME, Météo-France

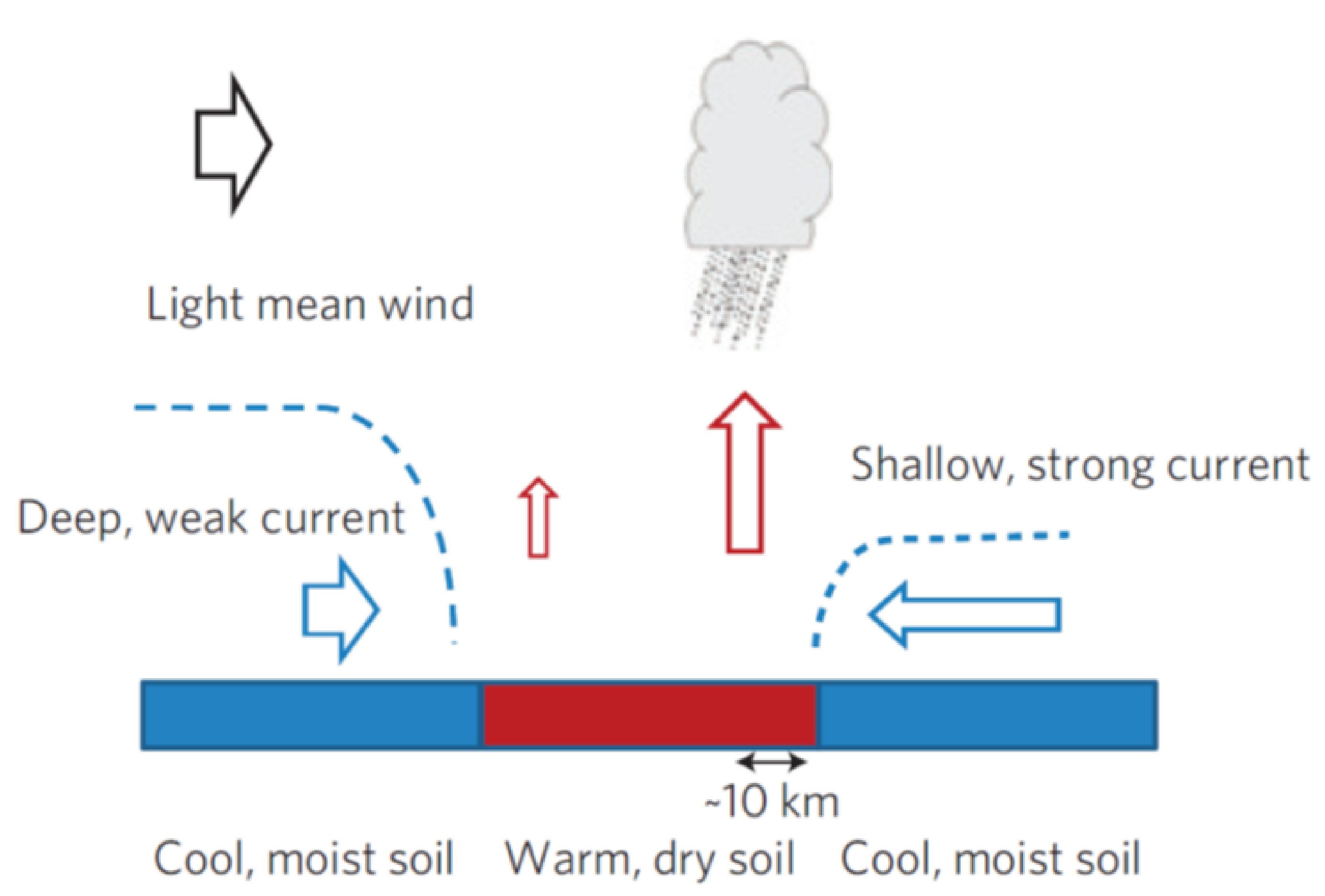

Figure 3.19: Schematic depicting the impact of soil-moisture heterogeneity on convective initiation. Idealized soil-moisture-induced flows (blue arrows) under light synoptic winds (black arrow) create an ascent region (large red arrow) where the shallow, strong current opposes the mean wind. The preferred location for convective initiation coincides with the ascent region induced by the heating gradient at the downwind edge of the dry patch. Additional convergence over the dry patch is provided by a deep, weaker current at its upwind edge, and cross-wind gradients in soil moisture .

(after Taylor et al., 2011; Reprinted by permission from Macmillan Publishers Ltd: [Nature Geoscience, 4, 430–433] (doi: 10.1038/ngeo1173), copyright (2011).

Chapter 3: ***Deep Convection*** **Lead Author: Jean Philippe Lafore, CNRM-GAME, Météo-France**

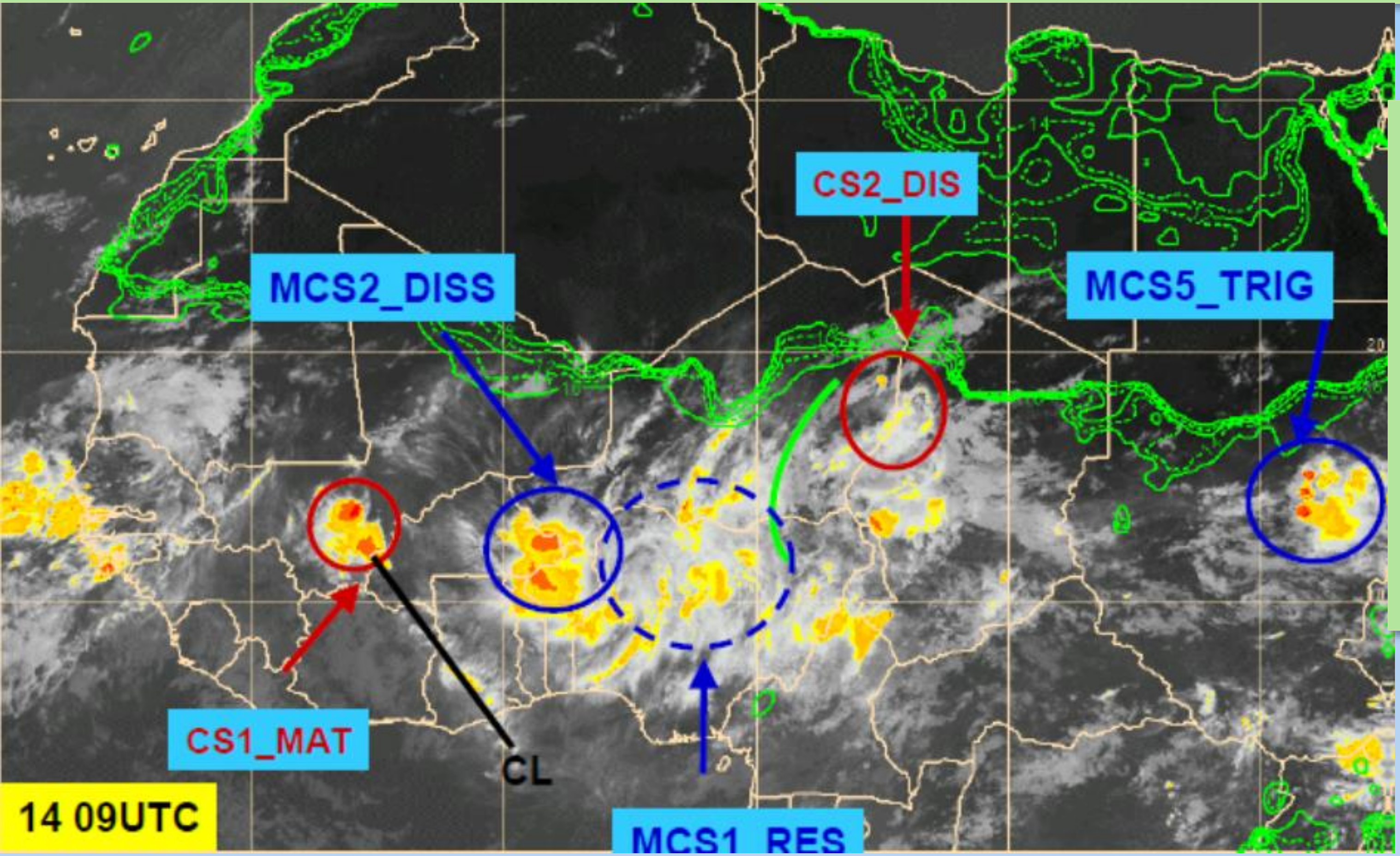

Figure 3.20/1: Illustration of the dissipation and triggering of some MCSs on the 14 August 2012, as extracted from the case study CS02 of an "Archetype of AEW" observed between the 13 to 16 August 2012.

Figure 3.20/1: IR Meteosat images at 09:00 UTC with yellow, red colours for coldest clouds (less than -40°C and -65°C respectively), and with green isolines of Td at 2 m every 2°C between 10°C and 16°C as provided by the ARPEGE operational analysis, to outline the ITD location. The main AEW trough is drawn with a green arc shaped line. The different MCS triggering, growing, mature, dissipation, residual and restart stages are labelled with the subscripts TRIG, GROW, MAT, DISS, RES and REST respectively.

Chapter 3: *Deep Convection* Lead Author: Jean Philippe Lafore, CNRM-GAME, Météo-France

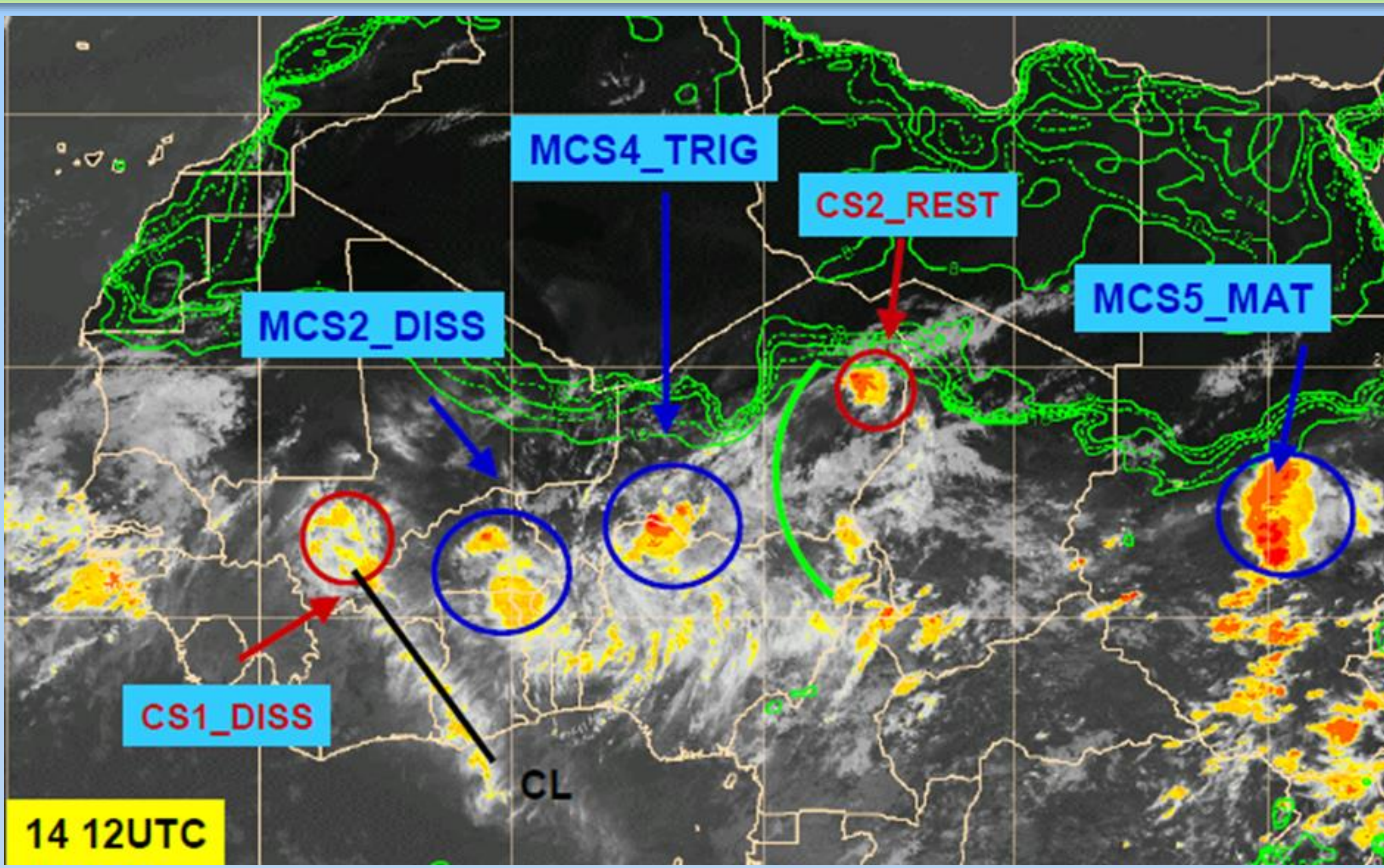

Figure 3.20/2: Illustration of the dissipation and triggering of some MCSs on the 14 August 2012, as extracted from the case study CS02 of an "Archetype of AEW" observed between the 13 to 16 August 2012.

Figure 3.20/2: IR Meteosat images at 12:00 UTC with yellow, red colours for coldest clouds (less than -40°C and -65°C respectively), and with green isolines of Td at 2 m every 2°C between 10°C and 16°C as provided by the ARPEGE operational analysis, to outline the ITD location. The main AEW trough is drawn with a green arc shaped line. The different MCS triggering, growing, mature, dissipation, residual and restart stages are labelled with the subscripts TRIG, GROW, MAT, DISS, RES and REST respectively.

Chapter 3: ***Deep Convection*** **Lead Author: Jean Philippe Lafore, CNRM-GAME, Météo-France**

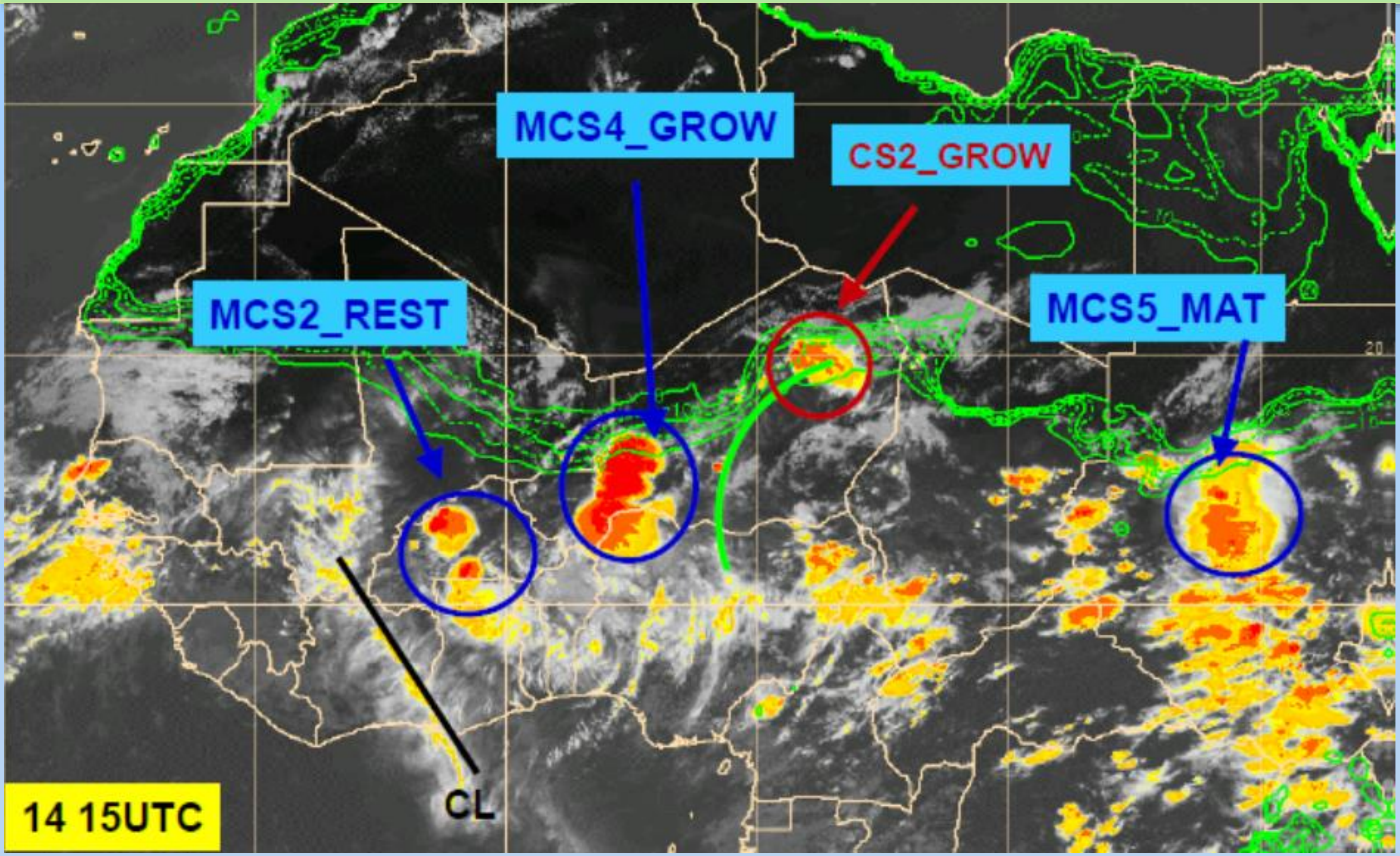

Figure 3.20/3: Illustration of the dissipation and triggering of some MCSs on the 14 August 2012, as extracted from the case study CS02 of an "Archetype of AEW" observed between the 13 to 16 August 2012.

Figure 3.20/3: IR Meteosat images at 15:00 UTC with yellow, red colours for coldest clouds (less than -40°C and -65°C respectively), and with green isolines of Td at 2 m every 2°C between 10°C and 16°C as provided by the ARPEGE operational analysis, to outline the ITD location. The main AEW trough is drawn with a green arc shaped line. The different MCS triggering, growing, mature, dissipation, residual and restart stages are labelled with the subscripts TRIG, GROW, MAT, DISS, RES and REST respectively.

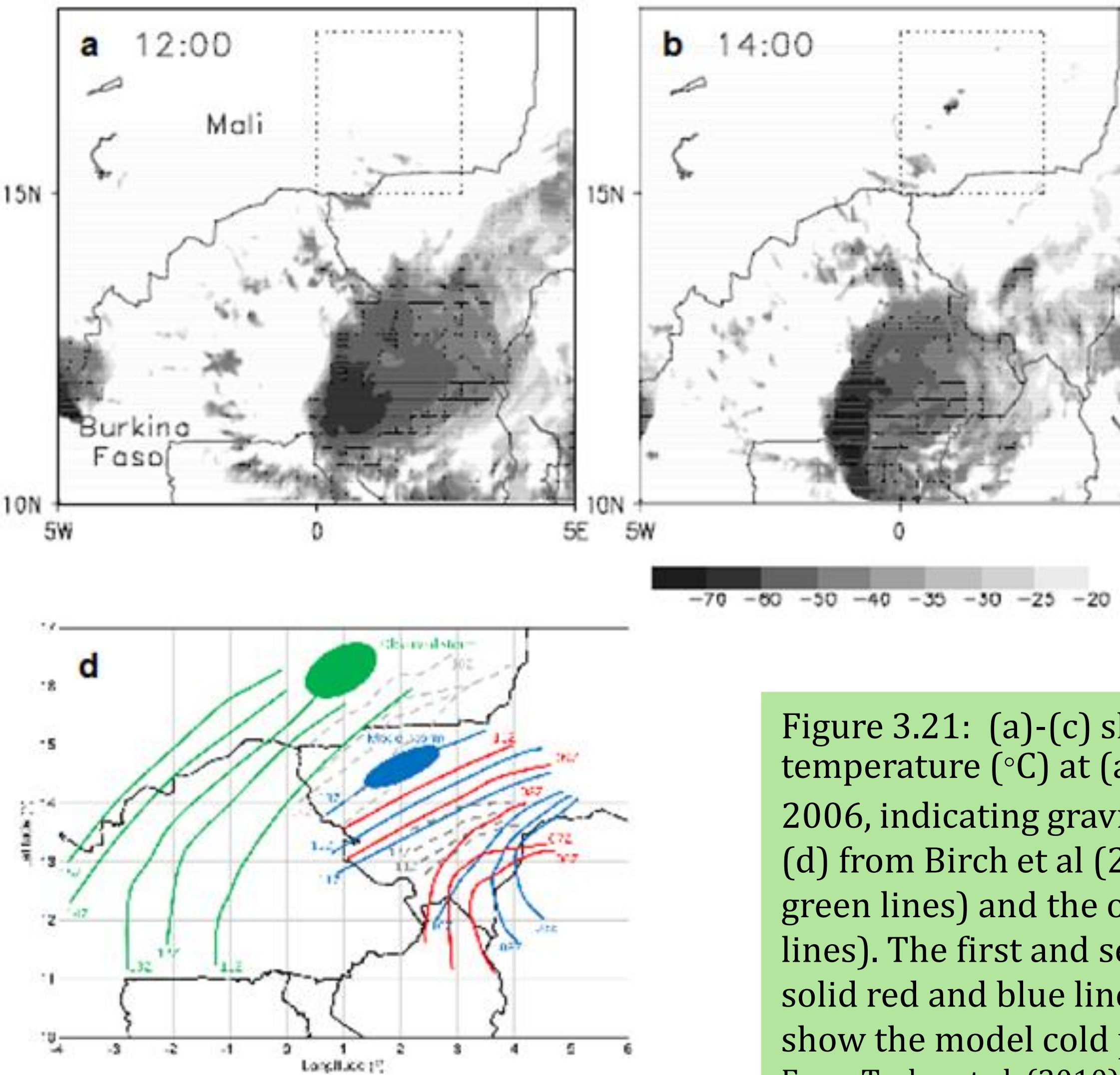

Figure 3.21: (a)-(c) showing cloud structures from brightness temperature (°C) at (a) 1200, (b) 1400 and (c) 1600 UTC, on 31 July 2006, indicating gravity-wave cloud and secondary initiation, and (d) from Birch et al (2013) showing observed gravity wave (solid green lines) and the observed cold pool (the light grey dashed lines). The first and second model gravity waves are shown by the solid red and blue lines respectively and the dark grey dashed lines show the model cold pool.
From Taylor et al. (2010)

African Monsoon Multidisciplinary Analysis

ACMAD

WMO

Chapter 3: *Deep Convection* Lead Author: Jean Philippe Lafore, CNRM-GAME, Météo-France

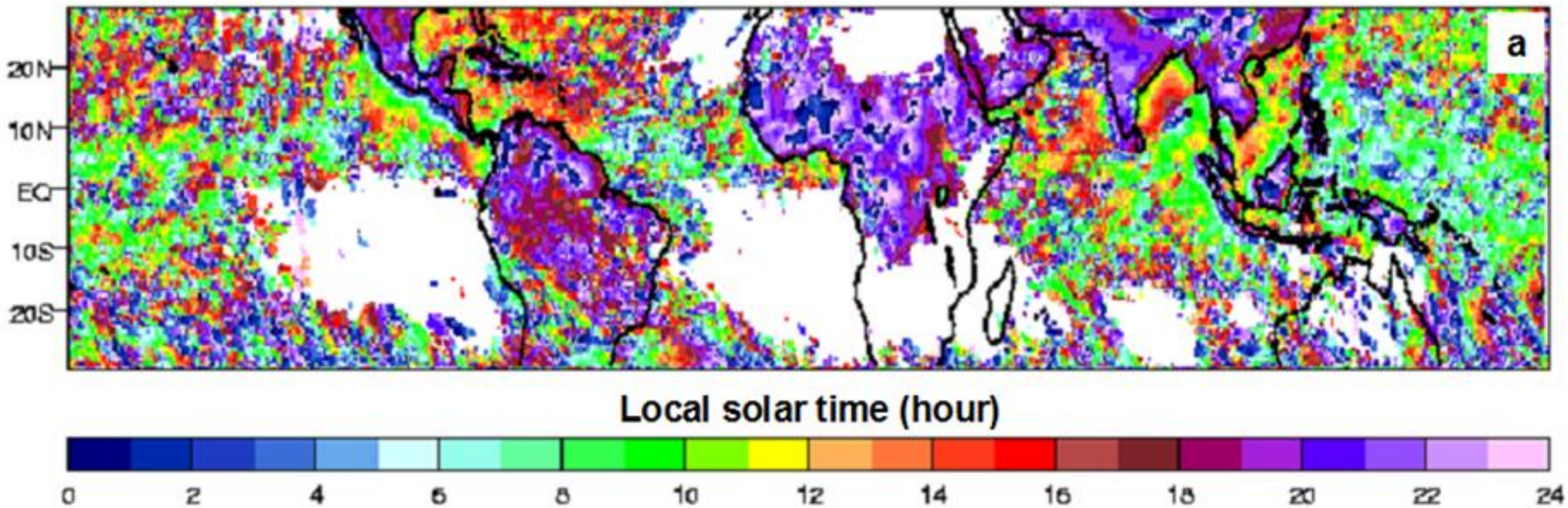

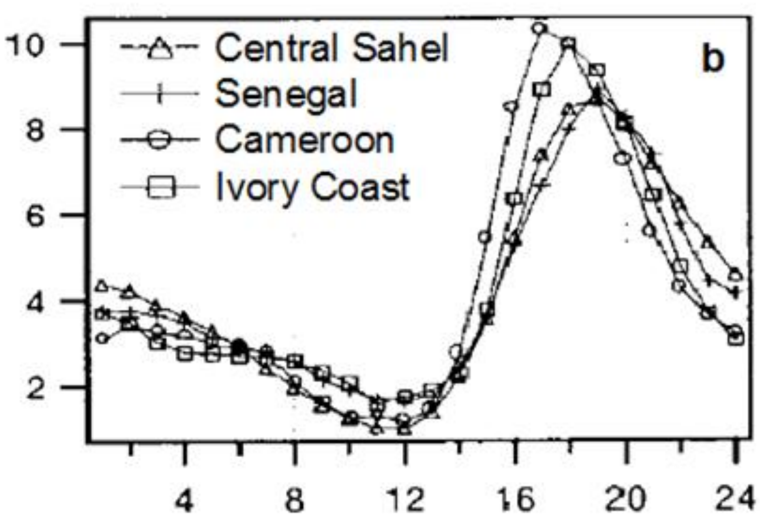

Figure 3.22: (a) Distribution of local time of the minimum of brightness temperature Tb from CLAUS (adapted by J-M. Piriou after Yang and Slingo, 2001) and (b) composite diurnal cycle of the fractional cloud cover (%) colder than 213◦K for 4 West African regions (after Mathon 2001 thesis).

African Monsoon Multidisciplinary Analysis

ACMAD

WMO

Meteorology of Tropical West Africa: The Forecasters’ Handbook

Chapter 3: *Deep Convection* Lead Author: Jean Philippe Lafore, CNRM-GAME, Météo-France

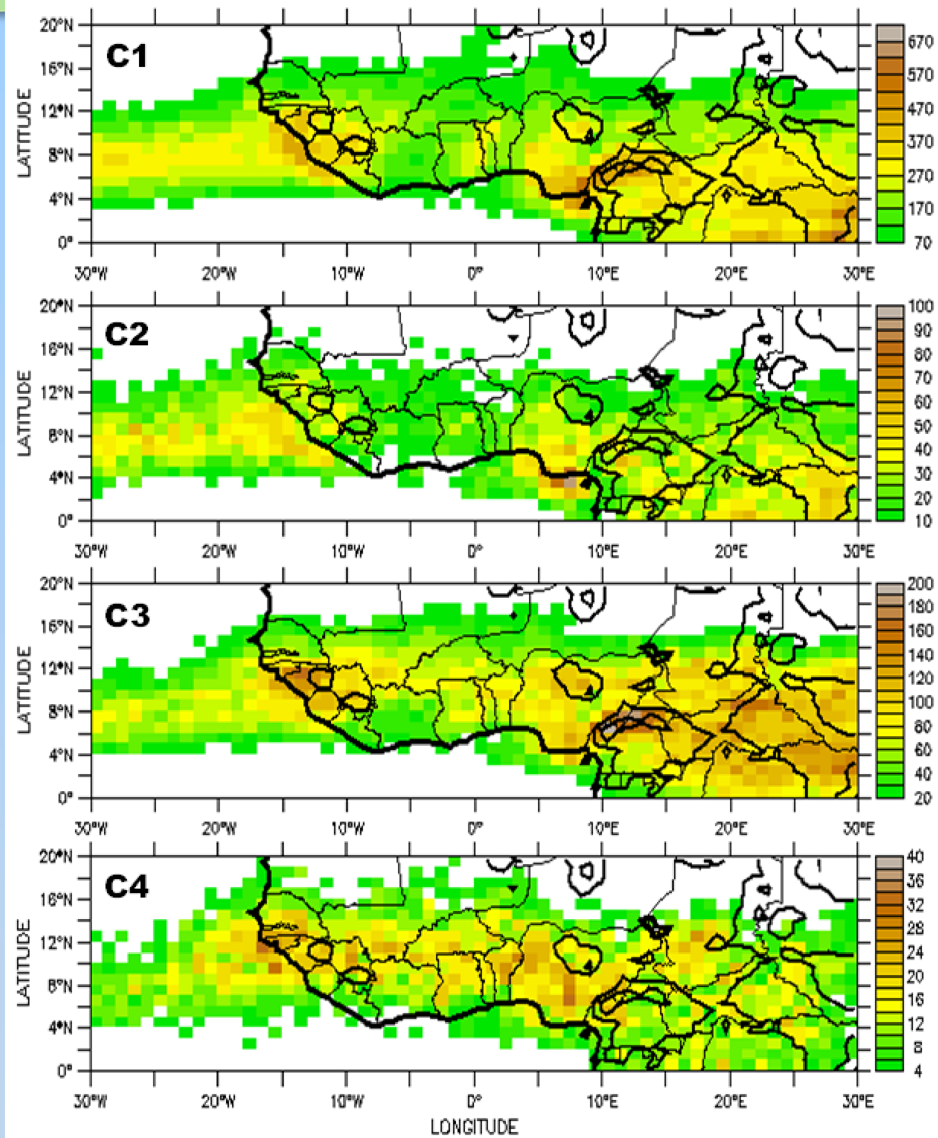

Figure 3.23: As for Figure. 3.16 for the location of the dissipation. Unit is the total number of triggering events over the 25-year period of the climatology.

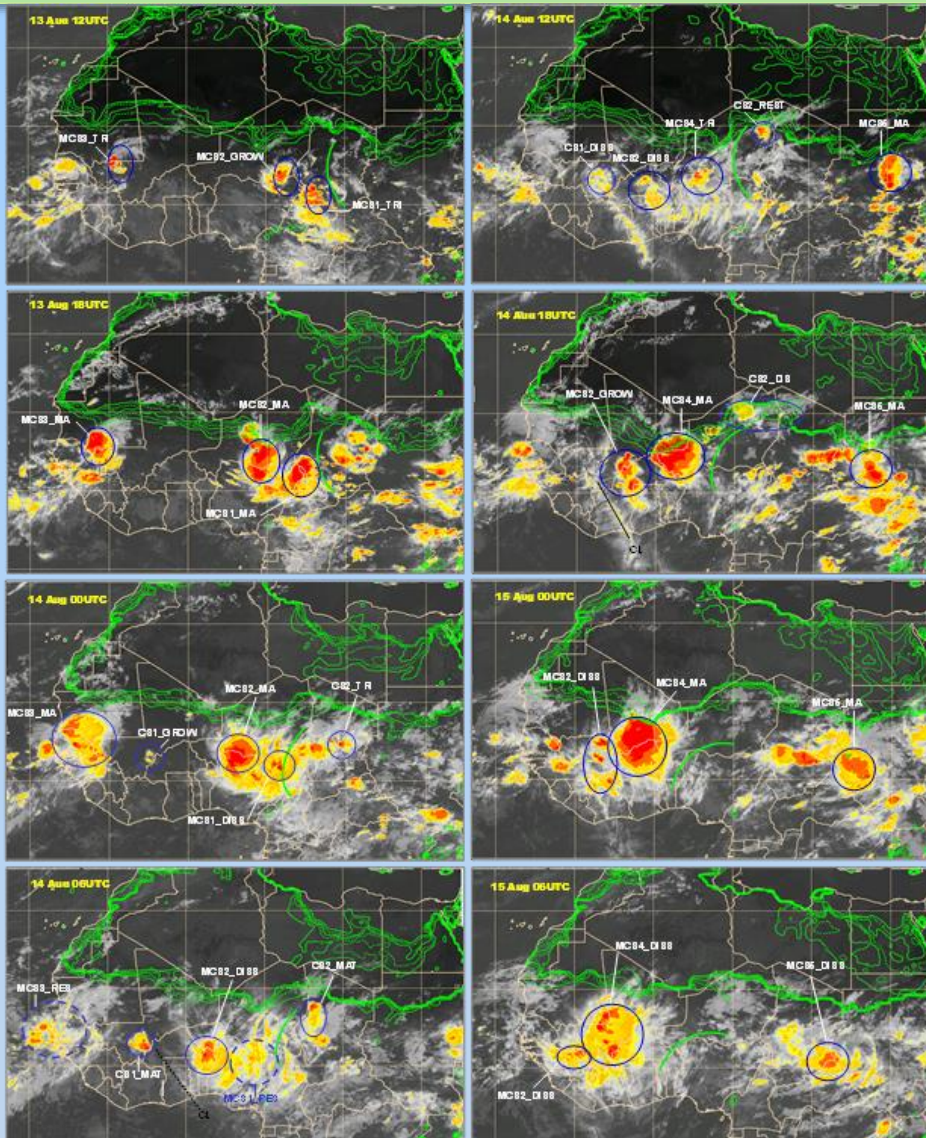

Figure 3.24: Sequence of images showing evolution of MCSs in CS02 showing at a 6 h frequency, IR Meteosat image with yellow, red colours for coldest clouds (less than -40°C and -65°C respectively), and with green isolines of Td at 2m every 2°C between 10°C and 16°C, to outline the ITD location. The main AEW trough is drawn with a green arc shaped line, and a convergence line is shown in black. The analysis is performed from the 13th at 1200 UTC to the 15th August at 1200 UTC. Convective Systems (CS) and Mesoscale Convective Systems (MCS) are numbered in their order of appearance, starting from the east, with a suffix corresponding to the stage of their life cycle: TRIG for the triggering stage; GROW for the growing stage; MA for the mature stage; DISS for the dissipation stage; RES for a convective residue; REST for a restart from a convective residue.

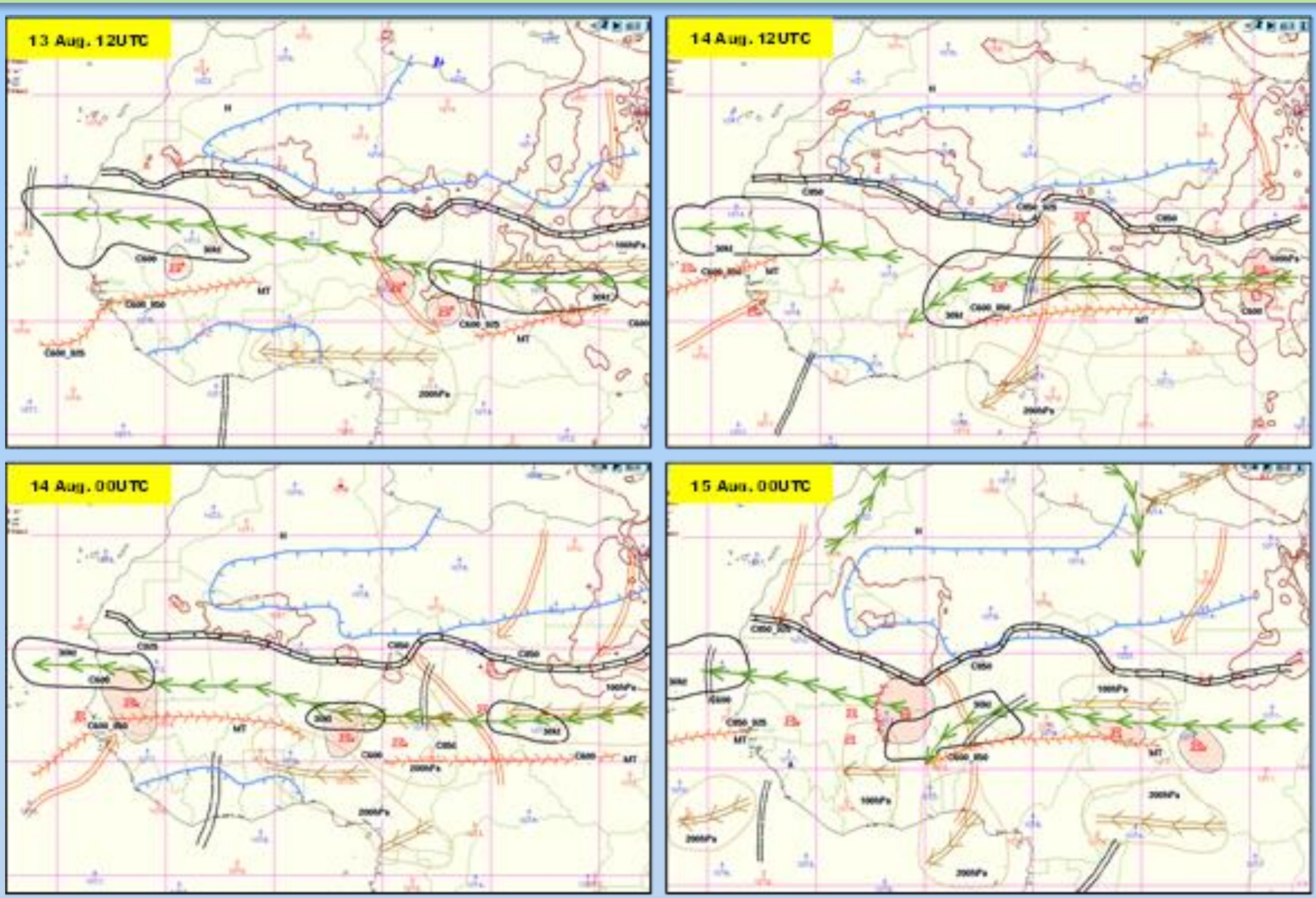

Figure 3.25: Sequence of WASA corresponding to the sequence of IR images of Figure 3.24 at a 12 h frequency.

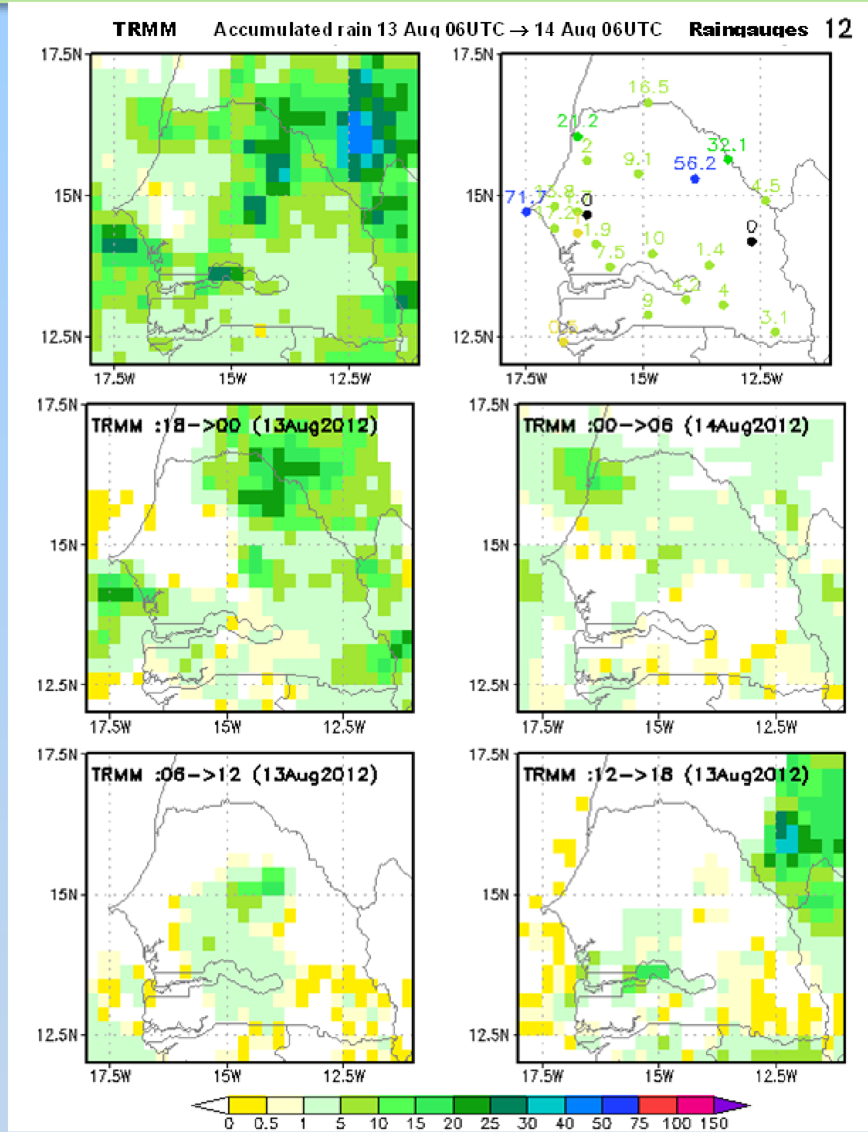

Figure 3.26: Precipitation over Senegal as estimated from TRMM and observed by the raingauge network between 0600 UTC on 13 August and 0600 UTC on 14 August , illustrating the footprint of MCS3.

African Monsoon Multidisciplinary Analysis

ACMAD

WMO

Meteorology of Tropical West Africa: The Forecasters' Handbook

Chapter 3: *Deep Convection* Lead Author: Jean Philippe Lafore, CNRM-GAME, Météo-France

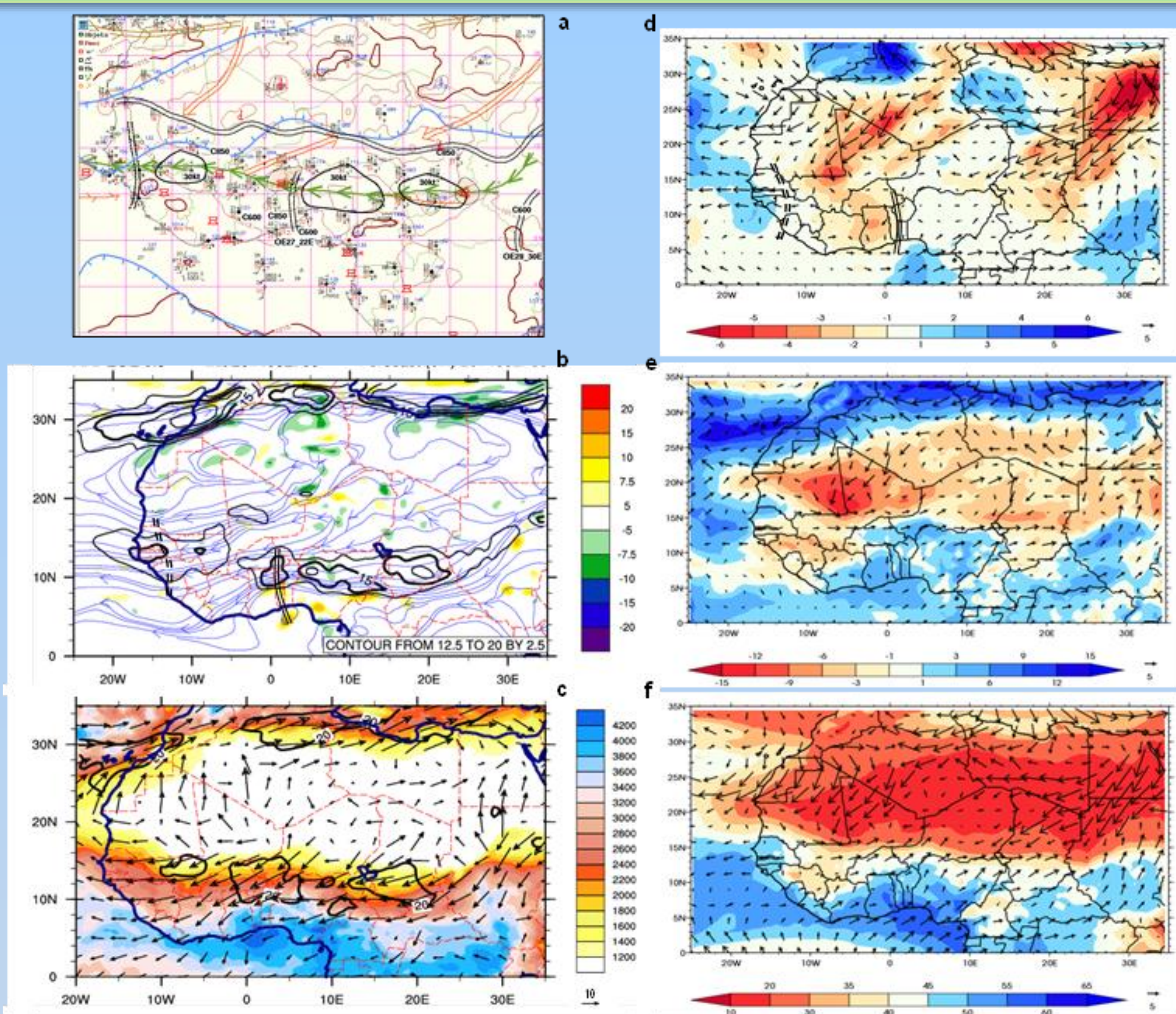

Figure 3.28: (a) WASA map on 17 September 2014 at 0600 UTC. The following panels are for the analysis at 0000 UTC. (b) Streamlines, wind intensity (thick black line above 15 ms-1) and vorticity (colour in 10-5 s-1) at 600 hPa. (c) Monsoon depth (colour in m) with wind shear vector (ms-1) in the 950-600 hPa layer, areas with shear larger than 20 ms-1 are outlined. (d) mean meridional in the 950-600 hPa layer (colour in ms-1) and mean wind vector in the 950-850 hPa layer. PW (colour) and wind vector at 950 hPa (ms-1) for (e) the anomaly and (f) total fields respectively.

Meteorology of Tropical West Africa: The Forecasters' Handbook
Editors: D J Parker and M Diop-Kane